JOURNAL OF GEOPHYSICAL RESEARCH, VOL. 101, NO. B4, PAGES 8271–8295, APRIL 10, 1996

Melting experiments on anhydrous peridotite KLB-1: Compositions of magmas in the upper mantle and transition zone

Claude Herzberg[1]
Department of Geological Sciences, Rutgers University, New Brunswick, New Jersey

Jianzhong Zhang
Center for High Pressure Research and Mineral Physics Institute, State University of New York at Stony Brook

Abstract. Electron microprobe results are reported for liquid and crystalline phases that were synthesized at 5–22.5 GPa in multianvil experiments on anhydrous peridotite KLB-1 [*Zhang and Herzberg*, 1994]. The results provide information on the partitioning of TiO_2, Al_2O_3, Cr_2O_3, FeO, MnO, MgO, Na_2O, and NiO among liquid and the crystalline phases olivine, modified spinel, garnet, magnesiowustite, and magnesium perovskite. Uncertainties in these partition coefficients stem from quenching problems and from the effects of thermal migration of liquid in a temperature gradient. We have, however, exploited the temperature gradients by determining how the crystalline phase chemistry varies throughout the melting interval from the liquidus to the solidus. This has permitted new constraints to be obtained on the compositions of liquids along the anhydrous peridotite solidus at low melt fractions and at pressures in the 5–18 GPa range. It is demonstrated that the wide range of Al_2O_3 and CaO/Al_2O_3 contents in picrites and komatiites can be explained by melt segregation at upper mantle pressures that ranged from 3 to ~10 GPa. These magmas could have formed by anhydrous melting in plumes with temperatures that were only 100°–200°C higher than ambient mantle below ridges, demonstrating that unusually hot conditions are not required to form komatiites. Primary igneous MgO contents in excess of 26% should be rare, and those that do exist in some komatiites can be explained by advanced melting during adiabatic or superadiabatic ascent, by low Na_2O in the source, or by melting in hot plumes from the transition zone and lower mantle. Evidence for deep melting in hot plumes is rather conjectural, but it may be contained in some 2700 Myr komatiites that have high MgO and mantle-like CaO/Al_2O_3.

Introduction

Zhang and Herzberg [1994] reported a new phase diagram for anhydrous peridotite KLB-1, based on a large number of melting experiments to 22.5 GPa, and a slightly modified version of this diagram is shown in Figure 1. These were multianvil experiments with an assembly configuration that generates a nonlinear temperature gradient from the hot spot to the cold end, an experimental method that was developed in Japan [*Ohtani*, 1979; *Ohtani et al.*, 1986; *Takahashi*, 1986; *Ito and Takahashi*, 1987] and subsequently adopted for melting experiments in other countries [*Kato et al.*, 1988a, b; *Gasparik*, 1989, 1990; *Herzberg et al.*, 1990; *Herzberg*, 1992; *Liebermann and Wang*, 1992; *Canil*, 1992; *Tronnes et al.*, 1992; *Presnall and Gasparik*, 1990; *McFarlane et al.*, 1994; *Zhang and Herzberg*, 1994].

The 15.5-GPa experiment shown in Figure 2 is fairly representative. When the melting temperature interval between the solidus and liquidus is substantial, the experiment develops the following hourglass structure: pockets of 100% quench liquid located near the hot spot; an assemblage of crystals ± quench liquid positioned between the solidus/liquidus melting interval; and an unmelted area at the cold end. The proportion of crystals/quench liquid contained within the solidus/liquidus melting interval is critically dependent on the temperature gradient and the time duration of the experiment. When both are low, there can exist a substantial amount of intercumulus liquid coexisting with its equilibrium crystalline assemblage [*Zhang and Herzberg*, 1994, Figures 4 and 5]. However, when both are high, liquid is expelled because of thermal migration (Figure 3), a solution and precipitation process that was originally reported at low pressures [*Lesher and Walker*, 1988]. When the melting interval between the solidus and liquidus is low, thermal migration is obviously inconsequential regardless of the size of the temperature gradient.

We have explored some of the effects of doing melting experiments in a temperature gradient by examining the crystalline and liquid phase chemistry with the electron microprobe. All liquid analyses refer to liquid quenched near the hot spot (Figure 2); analyses were also done on interculumus liquid in a 5-GPa experiment, but the results are of limited value because of extensive modification by quench olivine. Indeed, the effects of quenching on the liquid pockets near the hot spot can be larger than effects from thermal migration, and these are

[1]Also at Center for High Pressure Research and Mineral Physics Institute, State University of New York at Stony Brook.

Paper number 96JB00170.
0148-0227/96/96JB-00170$05.00

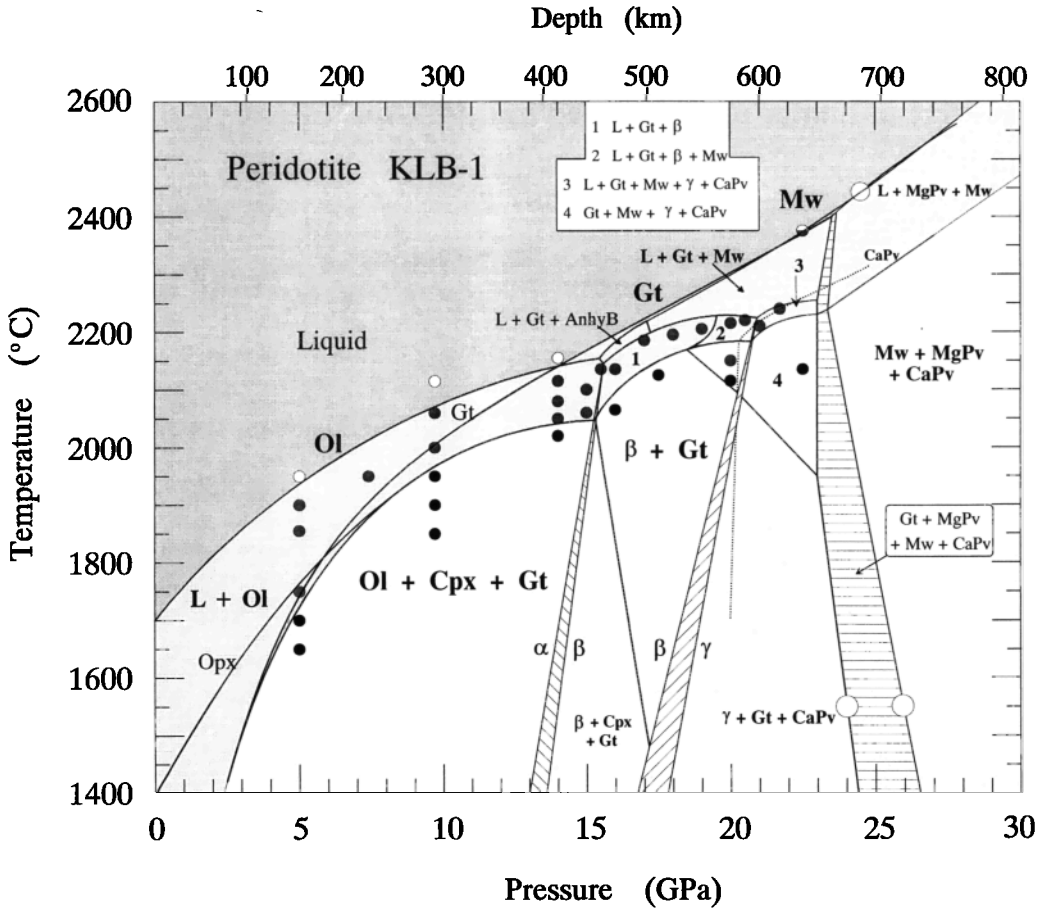

Figure 1. Phase diagram for anhydrous peridotite KLB-1, modified slightly from *Zhang and Herzberg* [1994]. Symbols are defined as follows: L, liquid; Ol, olivine; Opx, orthopyroxene; Cpx, clinopyroxene; Gt, garnet; AnhyB, anhydrous B; Mw, magnesiowustite; MgPv, magnesium perovskite; CaPv, calcium perovskite; α, olivine; β, modified spinel (Mg, Fe)$_2$SiO$_4$; γ, spinel (Mg, Fe)$_2$SiO$_4$. The original phase diagram has been modified in the following way: the perovskite-forming reaction has been placed at 23.5 GPa and solidus temperatures, based on the observations of majorite garnet at 22.5 GPa (this work) and perovskite at 24.5 GPa [*McFarlane et al.*, 1994] (open circle); a transition pressure wherein both majorite garnet and magnesium perovskite coexist has been included, based on experiments of *Irifune* [1994] (circles at 24–26 GPa and 1550°C); the solidus has been elevated by 100°C in the 20–22.5 GPa range (see text for details).

included as uncertainties in the analyses reported below. The crystalline phase immediately adjacent to the liquid pocket at the hot spot is the liquidus phase (Figure 3), and it will be shown that its chemistry changes appreciably down the temperature gradient. We have therefore exploited the temperature gradient by compiling a comprehensive database of analyses for crystalline phases that are distributed between the liquidus and the solidus; in many cases, this has enabled us to characterize both liquidus and solidus phase equilibria in a single experiment. Temperature gradients also promote equilibrium and homogeneity of crystalline phases owing to solution and precipitation [*Walker and Agee*, 1989; *Herzberg et al.*, 1990; *Zhang and Herzberg*, 1994].

About 1900 electron microprobe analyses covering 10 elements for 10 experiments in the 5–22.5 GPa range were acquired, and some of these results are reported here. On average, 200 crystal and liquid analyses were found to be the minimum number that is needed to provide a comprehensive description of how the phase chemistry varies along the temperature gradient for each experiment. Partition coefficients for major and trace elements between liquid and high-pressure crystalline phases have been determined, and this information has been used to place new constraints on the chemistry of liquids generated at low melt fractions on the anhydrous solidus.

Experimental Method

Melting experiments were performed on anhydrous mantle peridotite KLB-1 at 5–22.5 GPa using the multianvil press at the Center for High Pressure Research at Stony Brook. A comprehensive report of the experimental procedure was given by *Zhang and Herzberg* [1994], with special attention paid to precision and accuracy of temperature and pressure measurement, oxygen fugacity, equilibrium, temperature gradient, and the effects of temperature gradient on the phase diagrams.

Analytical Procedures

Experimental charges were mounted in epoxy, polished, examined with backscatter scanning electron microscopy (SEM), and the phases were analyzed with a JEOL 8600 electron

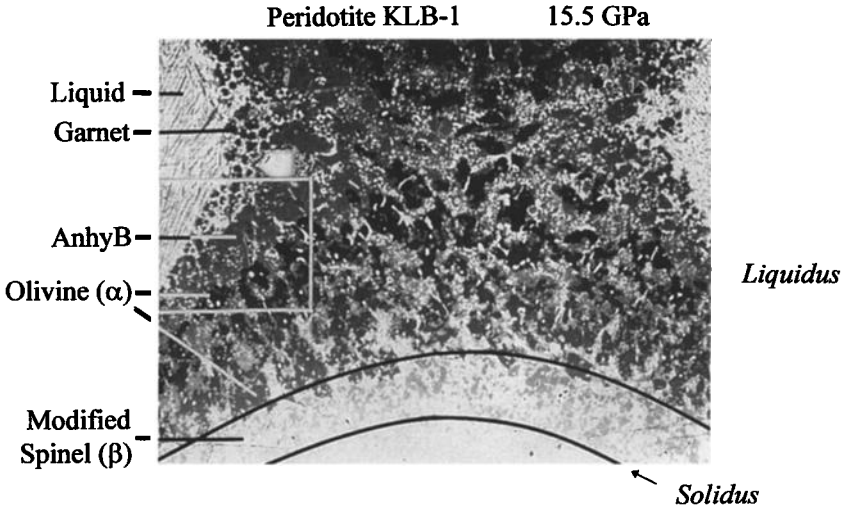

Figure 2. Backscatter SEM photomicrograph of an experiment at 15.5 GPa (KLB1-20 [*Zhang and Herzberg*, 1994]) showing a typical hourglass structure produced by the temperature gradient, with liquid (L) pockets defining the hot spot and unmelted portions of the charge at the cold end. Garnet (Gt) is distributed throughout from the liquidus to the solidus, and microprobe analyses are shown below. Crystallization sequence down the temperature gradient is L → L + Gt → L + Gt + AnhyB → L + Gt + Ol → L + Gt + Ol + β → L + Gt + β → [Gt + β]. Anhydrous B phase is $Mg_{12}Si_5O_{24}$.

microprobe at Rutgers University operating at an accelerating voltage of 20 keV. A beam current of 20 nA was employed for all elements. Counting times ranged from 5 to 24 s to obtain standard deviations of 1% on Si, Al, Fe, Mg, and Ca. Counting times of up to 40 s were required for Ti, Cr, Na, and Ni to obtain statistics that were within ±6%. Large standard deviations were often observed for Mn, and these data are of poor quality. Standards used were diopside for Si and Ca, pyrope for Al, pure forsterite for Mg, orthopyroxene for Fe, hornblende for Ti and Na, chromite for Cr, tephroite for Mn, and corning glass for Ni.

Crystalline phases were analyzed using a focused electron beam, but the melt phase was analyzed by rastoring an area because it quenches to a complex matrix of crystalline phases rather than a glass as shown in Figure 3. The rastoring was performed at a magnification of 8000X, and identical results were obtained for calibrations in both the spot and rastor mode; however, for calibrations in the spot mode, rastor analyses at magnifications of 4000X or less yielded totals that dropped to unacceptably low levels. Liquid analyses were repeated by rastoring at a magnification of 2000X with calibration in the rastor mode. Average liquid analyses for all oxides were virtually identical to those determined with the 8000X rastor, but rastoring at 2000X resulted in standard deviations that were lower for most oxides. In general, these lower standard deviations did not, however, propagate to a significant lowering of uncertainties in partition coefficients because of significant variations in the compositions of the crystalline liquidus phases; exceptions were standard deviations in the partition coefficients for magnesiowustite/liquid, which dropped by 50%.

A rastor analyses at 8000X provides an integrated composition of the quench crystalline matrix in an area of about 100 μm^2. About 20–40 analyses were made along a line transect, and usually two to four line segments were analyzed orthogonal and parallel to the liquidus isotherms; a total of 80–150 liquid analyses were obtained for each experiment, and the results are reported in Table 1. For both crystalline and quench liquid phases, only those analyses which totalled 100 ± 1% were accepted.

High-Pressure Phase Chemistry

Electron microprobe data presented are presented in Table 1. The average liquid analysis for each experiment is given as Lq1, and the variability about the mean is given as 1 standard deviation. This variability is random in the sense that it does not correlate with location along any of the line scans that were positioned orthogonal or parallel to the liquidus isotherms. The crystalline liquidus phases in Table 1 are those that only occur along the liquidus isotherm immediately adjacent to the hot spot, an example of which is given in Figure 3. Usually 15–30 analyses of the liquidus crystalline phase were obtained, with averages designated Ol1 or Gt1, and the parentheses indicate 1 standard deviation about the mean. The designation L1 and Gt1 therefore refers to the averages of the liquid and coexisting liquidus crystalline phase compositions; analyses designated L2 and Gt2 refer to individual analyses in each population that were the most refractory in terms of Fe/Mg, Ca/Al, Na, and Ti, a point discussed below.

The compositions of some representative coexisting crystalline phases positioned between the liquidus and solidus are also given in Table 1. At 15.5 GPa, for example, the compositions of coexisting olivine + anhydrous B + garnet are designated Ol3, AnhyB3, and Gt3. The absence of a liquid analysis with the same number indicates that these phases are positioned down the temperature gradient, and it is improper to compare them with liquid analyses L1 or L2. The change in crystalline phase chemistry down the temperature gradient is illustrated in Figures 4 to 9.

At 5 GPa the appearance of crystalline phases down the temperature gradient is L, Ol, Opx, Gt, Cpx (Figure 1; see discussion of this terminology by *Zhang and Herzberg* [1994]). The phases Opx, Gt, and Cpx are confined to the coldest part of these charges, and the crystalline assemblage immediately below the solidus is [Ol + Cpx + Gt]. Figure 4 shows that the

Table 1. Experimental Results

P, GPa	Phase	SiO_2	TiO_2	Al_2O_3	Cr_2O_3	FeO	MnO	MgO	CaO	Na_2O	NiO
5	Lq1	45.92 (0.32)	0.27 (0.02)	7.52 (0.32)	0.58 (0.03)	10.21 (0.15)	0.20 (0.10)	27.58 (0.97)	6.67 (0.34)	0.55 (0.03)	0.18 (0.03)
5	Ol1	41.07 (0.10)	0.01 (0.01)	0.20 (0.05)	0.20 (0.02)	6.52 (0.36)	0.10 (0.05)	51.41 (0.16)	0.21 (0.01)	0.02 (0.01)	0.36 (0.02)
5	Ol2	40.59 (0.30)	0.02 (0.02)	0.24 (0.03)	0.22 (0.04)	9.20 (0.24)	0.15 (0.07)	49.19 (0.38)	0.33 (0.02)	0.03 (0.01)	0.36 (0.01)
5	Opx2	55.69 (0.24)	0.02 (0.02)	3.37 (0.27)	0.52 (0.06)	4.77 (0.25)	0.09 (0.05)	32.88 (0.55)	2.11 (0.17)	0.18 (0.02)	0.15 (0.03)
5	Cpx2	54.64 (0.37)	0.05 (0.02)	3.75 (0.25)	0.42 (0.07)	5.37 (0.34)	0.15 (0.06)	26.50 (0.82)	8.07 (0.98)	0.60 (0.05)	0.11 (0.03)
5	Gt2	42.83 (0.26)	0.18 (0.03)	20.83 (0.37)	2.32 (0.14)	5.68 (0.16)	0.17 (0.08)	22.95 (0.54)	4.69 (0.35)	0.01 (0.01)	0.06 (0.02)
9.7	Lq1	46.14 (0.51)	0.14 (0.02)	4.42 (0.38)	0.44 (0.04)	9.39 (0.25)	0.14 (0.02)	34.21 (1.53)	3.68 (0.31)	0.38 (0.04)	0.22 (0.03)
9.7	Ol1	41.23 (0.13)	0.01 (0.01)	0.22 (0.01)	0.13 (0.02)	5.06 (0.01)	0.06 (0.04)	52.01 (0.40)	0.13 (0.02)	0.05 (0)	0.25 (0.01)
9.7	Gt2	46.98	0.05	17.58	1.1	4	0.08	27.5	2.6	0.02	0.06
9.7	Ol2	41.1	0.01	0.21	0.14	5.5	0.07	51.86	0.16	0.05	0.28
9.7	Gt3	46.12	0.28	16.34	1.2	7.08	0.15	24.52	4.5	0.12	0.07
9.7	Ol3	39.79	0.02	0.09	0.08	10.08	0.09	48.5	0.16	0.04	0.37
9.7	Cpx3	55.29	0.03	1.76	0.25	5.65	0.17	25.18	9.94	0.74	0.06
15.5	Lq1	44.96 (0.90)	0.14 (0.03)	2.96 (0.53)	0.35 (0.05)	10.06 (0.75)	0.15 (0.08)	37.12 (1.99)	3.66 (0.48)	0.33 (0.06)	0.25 (0.03)
15.5	Gt1	51.20 (0.44)	0.04 (0.02)	11.47 (0.73)	0.73 (0.05)	3.15 (0.17)	0.08 (0.06)	31.57 (0.29)	1.77 (0.22)	0.05 (0.01)	0.05 (0.01)
15.5	Lq2	44.3	0.12	3.54	0.38	8.59	0.14	39.5	3.03	0.3	0.21
15.5	Gt2	50.22	0.04	12.53	0.69	2.94	0.08	31.63	1.46	0.05	0.05
15.5	Gt3	51.77	0.05	9.85	0.78	3.66	0.09	31.04	2.23	0.06	0.07
15.5	Ol3	41.19	0.02	0.11	0.05	4.83	0.05	53.38	0.14	0.04	0.23
15.5	AnhyB3	33.08	0.04	1	0.41	6.41	0.25	58.12	0.03	0.04	0.46
15.5	Gt4	52.75	0.13	5.31	0.6	5.41	0.11	28.82	6.43	0.1	0.11
15.5	Bt4	40.01	0.06	0.48	0.19	9.48	0.09	47.97	0.1	0.04	0.57
18	Lq1	44.72 (1.13)	0.11 (0.03)	3.70 (0.46)	0.39 (0.04)	9.01 (0.84)	0.13 (0.03)	37.88 (1.55)	3.15 (0.58)	0.32 (0.07)	0.21 (0.03)
18	Gt1	51.79 (0.92)	0.05 (0.02)	9.64 (1.81)	0.61 (0.03)	3.14 (0.38)	0.06 (0.03)	32.46 (0.52)	1.93 (0.26)	0.06 (0.01)	0.06 (0.02)
18	Lq2	45.19	0.11	3.89	0.36	7.94	0.13	39.57	2.49	0.23	0.21
18	Gt2	50.3	0.05	12.09	0.6	2.67	0.06	32.02	1.58	0.06	0.06
18	Gt3	52.86	0.09	6.74	0.49	4.02	0.09	31.85	3.13	0.1	0.08
18	Bt3	40.48	0.03	0.7	0.19	6.31	0.1	52.11	0.07	0.02	0.35
18	Mw3	0.13	0.1	0.59	0.57	18.18	0.13	79.21	0.05	0.12	1.13
20	Lq1	45.67 (0.74)	0.13 (0.02)	3.26 (0.30)	0.36 (0.03)	9.47 (0.37)	0.15 (0.04)	36.34 (0.68)	3.38 (0.20)	0.37 (0.07)	0.21 (0.02)
20	Gt1	52.98 (0.46)	0.03 (0.01)	10.33 (0.75)	0.54 (0.02)	2.94 (0.17)	0.08 (0.01)	31.83 (0.31)	1.77 (0.09)	0.08 (0.01)	0.05 (0.01)
20	Mw1	0.16 (0.05)	0.00 (0.00)	1.01 (0.11)	0.64 (0.03)	15.05 (0.46)	0.12 (0.01)	81.84 (0.36)	0.00 (0.00)	0.13 (0.01)	0.86 (0.14)
20	Lq2	46.17	0.13	3.99	0.35	8.74	0.15	36.9	3.06	0.39	0.2
20	Gt2	52.44	0.03	11.01	0.52	2.93	0.08	31.55	1.69	0.08	0.05
20	Mw2	0.16	0	1.1	0.64	14.68	0.12	82.52	0	0.13	0.86
20	Gt3	55.27	0.09	5.09	0.43	4.07	0.12	32.18	2.67	0.12	0.07
20	Bt3	41.45	0.02	0.41	0.17	6.59	0.07	50.84	0.05	0.06	0.37
20	Gt1	54.24 (0.37)	0.12 (0.02)	5.02 (0.47)	0.41 (0.07)	4.55 (0.21)	0.11 (0.04)	31.87 (0.93)	3.65 (0.95)	0.21 (0.02)	0.07 (0.05)
20	Bt1	41.14 (0.38)	0.02 (0.02)	0.36 (0.03)	0.10 (0.04)	7.70 (0.29)	0.07 (0.03)	50.27 (0.51)	0.04 (0.02)	0.10 (0.02)	0.32 (0.04)
20	Mw1	0.25 (0.32)	0.04 (0.02)	0.40 (0.09)	0.41 (0.04)	21.70 (1.23)	0.14 (0.04)	75.31 (1.84)	0.09 (0.04)	0.27 (0.03)	1.06 (0.06)
21.7	Lq1	45.30 (0.35)	0.11 (0.02)	3.84 (0.29)	0.40 (0.03)	8.57 (0.43)	0.13 (0.03)	36.51 (0.34)	3.11 (0.19)	0.27 (0.04)	0.23 (0.02)
21.7	Gt1	53.51 (0.89)	0.03 (0.01)	8.50 (1.32)	0.51 (0.03)	3.09 (0.24)	0.09 (0.02)	32.60 (0.26)	2.03 (0.24)	0.08 (0.01)	0.05 (0.01)
21.7	Mw1	0.15 (0.01)	0.01 (0.02)	1.32 (0.06)	0.62 (0.02)	13.43 (0.24)	0.12 (0.14)	83.15 (0.33)	0.04 (0.01)	0.16 (0.07)	0.90 (0.03)
21.7	Lq2	45.12	0.11	4.45	0.45	7.69	0.13	37.43	2.71	0.21	0.23
21.7	Gt2	52.23	0.03	10.04	0.50	2.83	0.09	32.31	1.71	0.08	0.05
21.7	Mw2	0.15	0.01	1.36	0.61	12.97	0.12	83.59	0.04	0.13	0.9
22.5	Lq1	46.64 (0.57)	0.09 (0.02)	4.41 (0.34)	0.40 (0.03)	7.13 (0.51)	0.11 (0.04)	37.11 (0.59)	2.83 (0.22)	0.23 (0.04)	0.22 (0.07)
22.5	Gt1	53.36 (0.99)	0.04 (0.02)	8.19 (1.40)	0.44 (0.03)	2.73 (0.28)	0.10 (0.10)	32.82 (0.45)	2.00 (0.31)	0.09 (0.04)	0.07 (0.04)
22.5	Mw1	0.18 (0.02)	0.02 (0.02)	1.55 (0.07)	0.59 (0.02)	10.92 (0.20)	0.12 (0.11)	85.79 (0.46)	0.04 (0.01)	0.11 (0.03)	0.87 (0.02)
22.5	Lq2	46.79	0.09	5.04	0.45	6.17	0.11	37.61	2.5	0.16	0.22
22.5	Gt2	52.36	0.04	11.03	0.42	2.24	0.05	33.08	1.54	0.08	0.07
22.5	Mw2	0.18	0.02	1.51	0.58	10.69	0.08	85.53	0.04	0.1	0.87

Numbers in parentheses are 1 standard deviation of averages. Phases with common numbers are coexisting phases. Lq, liquid; Ol, olivine; Opx, orthopyroxene; Cpx, clinopyroxene; Gt, garnet; AnhyB, anhydrous B; Bt, beta phase (modified spinel); Mw, magnesiowustite. Nominal temperatures of these experiments are given by *Zhang and Herzberg* [1994].

FeO content of olivine varies systematically from about 4.5% at the liquidus to about 9.5% near the solidus. Quench liquid analyses obtained from the vicinity of the hot spot display complementary FeO-MgO relations and are roughly similar to liquids formed by about 70–100% melting of KLB-1 except that they are displaced to lower contents of FeO. The calculated liquid compositions were determined from the partition coefficients as discussed below and from the topologies of the liquidus crystallization fields at 5 GPa [*Herzberg*, 1992, 1993a, b], and these should be similar to liquids expelled by thermal migration. However, the match between observed and calculated liquid compositions is poor, and much of the variability is actually due to olivine which forms large dendritic crystals having about 7% FeO upon quenching during the termination

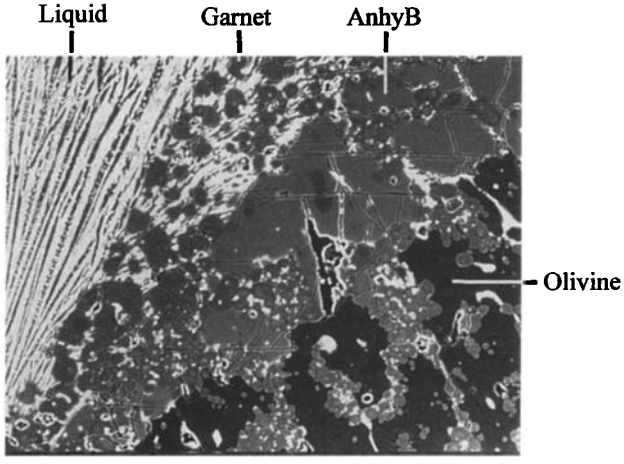

Figure 3. Magnified view of 15.5-GPa experiment shown in Figure 2, also from *Zhang and Herzberg* [1994]. Liquidus garnets refer to only those garnets that are distributed immediately adjacent to the liquid pockets at the hot spot.

of the experiment. A pocket of liquid near the capsule wall and at the cold end was found to have much smaller quench crystals and it yielded much better statistics (Table 1), and it is similar to a liquid produced by about 50% melting of KLB-1. Figure 4 shows that liquids formed by degrees of melting lower than about 50% were either not expelled by thermal migration, or they were mixed with higher-degree melts.

Similar observations are made at 9.7 GPa, and this is shown in Figure 5. Liquids quenched near the hot spot are similar to liquids produced by 70–100% melting of KLB-1, except that they are displaced to lower FeO than those expected from thermal migration; most of the scatter is due to quench olivine.

The experiments at 15.5 GPa are particularly interesting because the liquidus phase is garnet, the olivine (α) to modified spinel (β) transformation is clearly visible (Figures 2 and 3), and there are only two crystalline phases in the subsolidus, these being modified spinel + garnet. Figure 6 shows that garnets display a wider range of chemistries than at lower pressures, and this reflects the stabilization of garnet throughout the entire melting interval. There exists a noticeable break in FeO-MgO at the $\alpha - \beta$ transformation as expected from other studies [e.g., *Katsura and Ito*, 1989]. Again, liquids at the hot spot are similar to liquids formed by about 70–100% melting of KLB-1, and there is more scatter in FeO and MgO due to thermal migration rather than to quenching. For CaO and Al_2O_3 there is more scatter from quenching than from thermal migration (Figure 7).

The compositions of modified spinel and garnet immediately below the solidus at 15.5 GPa can be calculated from the partitioning of elements between these two phases as discussed below together with the constraint of mass balance, and these calculated compositions can be compared to those which are directly observed. Figure 6 shows that the agreement is very good, but the observed compositions of β and Gt are somewhat more FeO-rich than expected. Figure 7 also shows that the observed garnets are somewhat higher in CaO and lower in Al_2O_3 than garnets which are required for mass balance. Mass

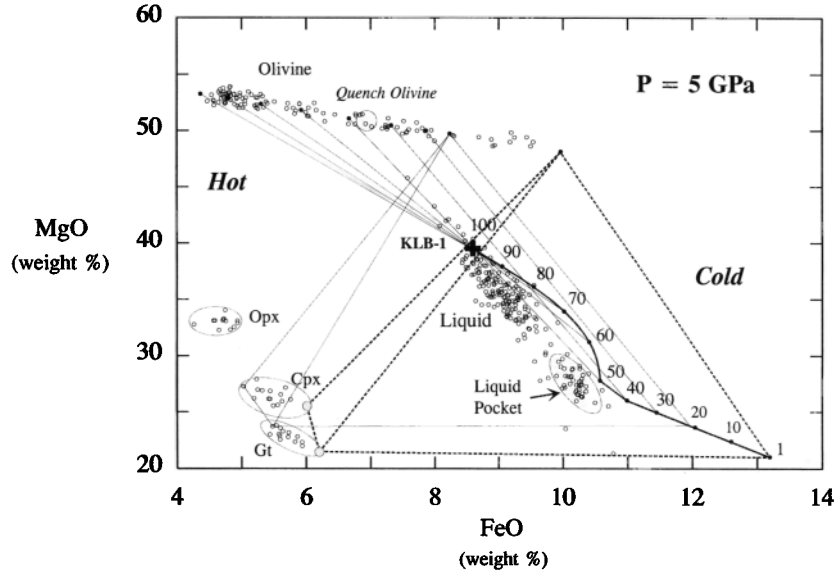

Figure 4. FeO and MgO of phases contained in a 5 GPa experiment, KLB1-28 of *Zhang and Herzberg* [1994]. Olivine displays a continuum of compositions from low FeO near the hot spot to high FeO at the cold end. Bold solid curve represents the compositions of liquids formed by 1 to 100% melting of KLB-1: [L + Ol + Opx + Cpx + Gt at 1 to 22% melting]; [L + Ol + Opx + Gt at 22 to 40% melting]; [L + Ol + Opx at 40 to 50% melting]; [L + Ol at 50 to 100% melting]. Liquid compositions were calculated from partition coefficients as described in the text and from the topologies of the liquidus crystallization fields at 5 GPa [*Herzberg*, 1992, 1993a, b]. Compositions of coexisting phases at the solidus are given in Table 3 and are represented as bold dashed tie lines; these differ from observed phase compositions by several tenths of a weight percent and were estimated by regression and mass balance. Fine solid lines tie coexisting phases within the melting interval. The "liquid pocket" is a segregated pocket of liquid along the capsule wall at the cold end and contains small rather than large quench crystals; analyses are given in Table 1.

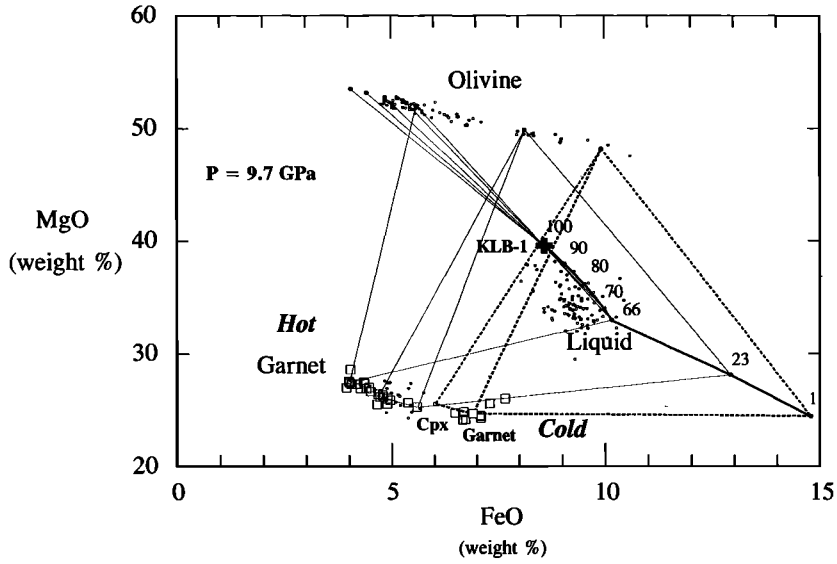

Figure 5. FeO and MgO of phases contained in a 9.7-GPa experiment, KLB1-30 of *Zhang and Herzberg* [1994]. Bold solid curve represents the compositions of liquids formed by 1 to 100% melting of KLB-1: [L + Ol + Gt + Cpx at 1 to 23% melting]; [L + Ol + Gt at 23 to 66% melting]; [L + Ol at 66 to 100% melting]. Compositions of coexisting phases on the solidus are given in Table 3. Other conventions are as for Figure 4, except compositional similarities between garnet and clinopyroxene are distinguished by squares (garnet) and small circles (Cpx).

balance is therefore not strictly achieved at the cold end of these experiments, and the departure from mass balance increases at higher pressures.

At 18 GPa the solidus mineralogy is also [β + Gt], and the observed phases are marginally enriched in FeO compared with the calculated ones (Figure 8). Again, liquid analyses display variations in FeO and MgO that appear to be dominated by thermal migration, and variations in CaO and Al_2O_3 are due mainly to quench effects.

Differences between calculated and observed phase chemistries at the solidus increase systematically from 20 to 22.5 GPa (Figure 9). Magnesiowustite becomes an important crystallizing phase, and it is stable in the subsolidus (β + Gt + Mw at 20 GPa; γ + Gt + Mw + CaPv at 21.7 to 22.5 GPa; Figure 1). At 21.7 GPa, magnesiowustite can have up to 50% FeO (Figure 9), and the high FeO contents of coexisting γ and Gt would indicate that the bulk FeO has increased from 8.59% (i.e., the value in KLB-1) to over 15%. It is also noteworthy that for any specified garnet composition at the cold end, the calculated FeO contents of equilibrium magnesiowustites are always lower than those which are observed. These differences most likely arise from important nonideal terms [*Fei et al.*, 1991] that were not considered for the more FeO rich Gt-Mw pairs (see below). The experiments in the 20–22.5 GPa range were run with a smaller tungsten carbide truncation, and the temperature gradients in them are larger than those at 15.5 GPa. The systematic increases in FeO concentrations in the cold end are therefore most likely to be an artifact of higher-temperature gradients rather than higher pressures.

In addition to FeO, crystalline assemblages at the cold end display enrichments in TiO_2, CaO, and SiO_2 and strong depletions in Al_2O_3; also at the cold end, Na_2O is enriched at 21.7–22.5 GPa, but it is depleted at lower pressures. These changes in chemistry are somewhat similar to those that would be expected from the migration of liquids to the cold end, and since FeO migrates from low to high concentrations, the process is similar to uphill diffusion. However, FeO also diffuses from high to low temperatures, and this differs from previous reports of uphill diffusion which have been isothermal cases [*Zhang et al.*, 1989; *Chakraborty et al.*, 1995]. Soret experiments run at 1 GPa on a basalt composition yield at the cold end of the temperature gradient enrichments in FeO, CaO, TiO_2, and MgO and depletions in Na_2O and SiO_2; Al_2O_3 remains relatively constant [*Walker and DeLong*, 1982; *Lesher and Walker*, 1986]. We see similarities (i.e., CaO, FeO, TiO_2), but the differences (i.e., SiO_2, Al_2O_3, and MgO) could arise from higher-temperature gradients in our experiments, higher pressures, different bulk compositions, or a diffusion mechanism that differs from Soret diffusion. In the absence of a satisfactory understanding, we use the term cold-directed thermal migration to describe the enrichments and depletions at the cold end.

The cold-directed thermal migration process has so effectively transformed the bulk composition of our system at the cold end in the pressure range 20–22.5 GPa that this has resulted in two important ambiguities of interpretation made by *Zhang and Herzberg* [1994]. Once melting begins the diffusion of FeO to the cold end will surpress the melting temperature, and this explains problems we had at bracketing the solidus at 20 GPa: at 2115°C no liquid phase was observed anywhere in the charge, but at 2150°C we observed a melt fraction that was much greater than that expected by a 35°C increase in temperature [*Zhang and Herzberg*, 1994]. The solidus temperatures in our new phase diagram in Figure 1 have therefore been elevated by about 100°C at 22.5 GPa.

Another difficulty caused by cold-directed thermal migration in our 22.5-GPa experiment was the absence of spinel (γ) (Mg, Fe)$_2SiO_4$ at any position within the melting interval. We originally interpreted the absence of spinel to indicate the stability of perovskite from the well-known reaction (Mg, Fe)$_2SiO_4(\gamma)$

= (Mg, Fe)SiO_3 (perovskite) + (Mg, Fe)O (magnesiowustite) [*Zhang and Herzberg*, 1994]. We have since examined this experiment more carefully and have found (γ) (Mg, Fe)$_2SiO_4$ at the coldest part of the charge where there was no liquid phase. The effect of FeO diffusion was to remove the bulk composition from [γ + Gt + Mw] space to [Gt + Mw]. We erroneously identified garnet as perovskite and have confirmed this error by micro-Raman analysis. To the untrained eye, our new phase diagram for KLB-1 in Figure 1 will look identical to the old one, but we have now placed the perovskite-forming reaction 1 GPa higher in pressure. *McFarlane et al.* [1994] identified perovskite in a melting experiment at 24.5 GPa and on a composition that is very similar to KLB-1. Majorite garnet is stable in our experiments at 22.5 GPa, and this permits us to place the perovskite-forming reaction between these two brackets, at 23.5 GPa and at temperatures between the solidus and liquidus (Figure 1). Additional experimental work would be desirable to constrain the T-P location of this important transformation.

Crystal/Liquid Partitioning

General Information

It is now possible to evaluate the partitioning of the elements TiO_2, Al_2O_3, Cr_2O_3, FeO, MnO, MgO, CaO, Na_2O, and NiO between crystals and liquid. We have adopted the convention of *Beattie et al.* [1993] where the partitioning of cation M between phases X and Y takes the form

$$D_{MO}^{X/Y} = C_{MO}^{X}/C_{MO}^{Y} \quad (1)$$

where C represents the weight fraction of the metal oxide component MO in the phases X and Y. For crystal/liquid pairs, phase X refers to the crystalline phase and phase Y to the liquid phase, so that

$$D_{MO}^{X/Y} = D_{MO}^{Xtl/Lq} \quad (2)$$

but we show our results explicitly as, for example,

$$D_{MgO}^{Xtl/Lq} = [MgO]^{Xtl}/[MgO]^{Lq} \quad (3)$$

where $[MgO]^{Xtl}$ is the weight percent concentration of MgO in the crystalline phase (Xtl). To calculate the composition of a crystalline phase from a known liquid composition, it is more convenient to consider the partition coefficients on a molar

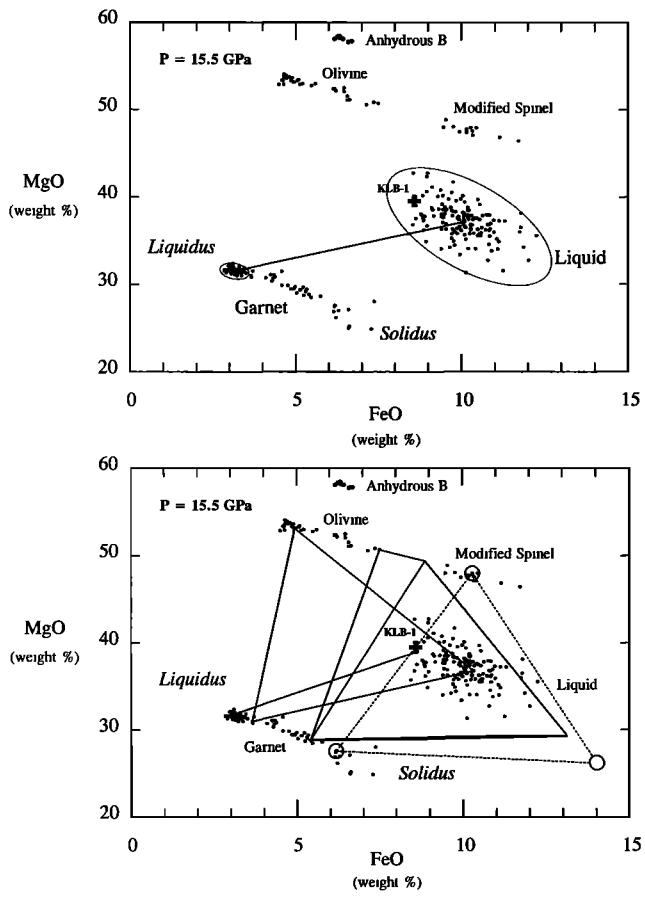

Figure 6. FeO and MgO of phases contained in a 15.5 GPa experiment, KLB1-20 of *Zhang and Herzberg* [1994]. Liquidus garnets and quench liquid shown in Figure 3 have analyses indicated in the top panel; averages and standard deviations are given in Table 1. Coexisting garnet, olivine, modified spinel, and calculated liquids along the temperature gradient of Figure 2 are indicated by tie lines. Dashed lines tie solidus phases.

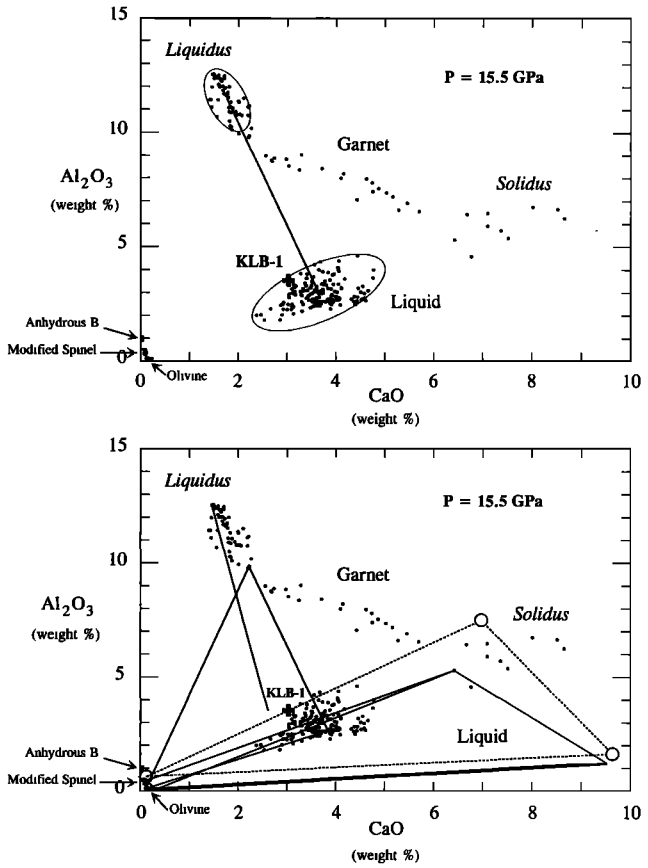

Figure 7. Al_2O_3 and CaO of phases contained in the 15.5-GPa experiment, KLB1-20. Garnets display a continuum of compositions from high Al_2O_3 at the liquidus to low Al_2O_3 near the solidus. Liquidus garnets and quench liquid shown in Figure 3 have analyses indicated in top panel; averages and standard deviations are given in Table 1. Coexisting garnet, olivine, modified spinel, and calculated liquids along the temperature gradient of Figure 2 are indicated by tie lines. Dashed lines tie solidus phases. Liquid analyses scatter in two compositional vectors, one defined by thermal migration at approximately constant Al_2O_3, the other by quench olivine and garnet, which is the dominant effect as shown by the major axis of the ellipse.

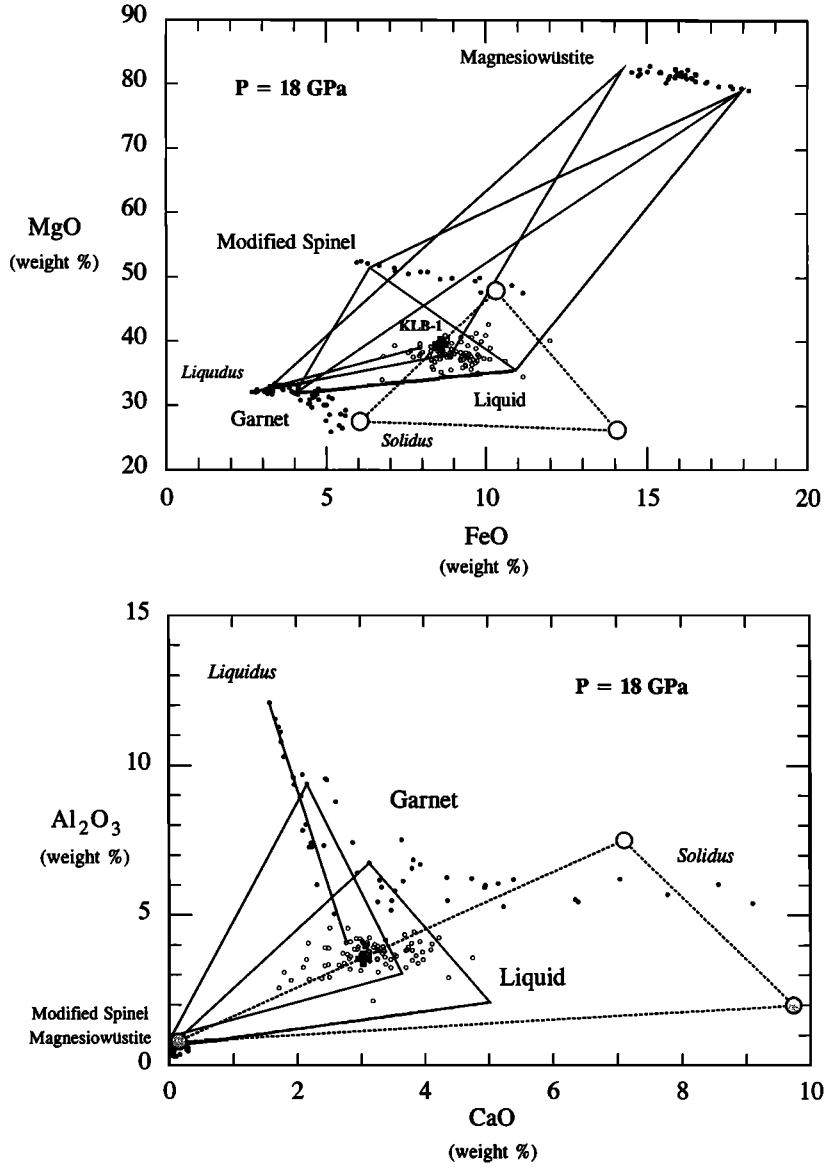

Figure 8. (top) FeO and MgO and (bottom) Al_2O_3 and CaO of phases contained in an 18-GPa experiment, KLB1-10 of *Zhang and Herzberg* [1994]. The crystallization sequence down the temperature gradient is L → L + Gt → L + Gt + Mw → L + Gt + Mw + β → L + Gt + β → [Gt + β]. Analyses of representative phases are given in Table 1.

basis rather than a weight percent basis; conversion factors for various crystalline phases are given in Table 2.

For peridotite KLB-1, olivine is the liquidus phase below 14 GPa, garnet is the liquidus phase above 14 GPa, and KLB-1 is multiply saturated in both at this pressure (Figure 1). The partitioning of FeO for olivine/liquid at $P < 14$ GPa and for garnet/liquid at $P > 14$ GPa can be evaluated in a straightforward manner from our electron probe data in Table 1, and this is shown in Figure 10 together with results for MgO. However, partition coefficients are also shown for modified spinel/liquid even though modified spinel is never a liquidus phase and it never coexists with easily analyzable pockets of liquid because it found down the temperature gradient towards the colder ends of the capsules (e.g., Figure 2). These were calculated from the thermodynamic constraint

$$D_{FeO}^{\beta/Lq} = D_{FeO}^{Gt/Lq} D_{FeO}^{\beta/Gt}, \quad (4)$$

where $D_{FeO}^{Gt/Lq}$ is known and the compositions of coexisting garnet and modify spinel in Table 1 permit an evaluation to be made of $D_{FeO}^{\beta/Gt}$. Similarly, at pressures lower than 14 GPa where olivine is the liquidus phase, partition coefficients for garnet/liquid were calculated from the relation

$$D^{Gt/Lq} = D^{Ol/Lq} D^{Gt/Ol} \quad (5)$$

where $D^{Ol/Lq}$ is known and $D^{Gt/Ol}$ is determined from the compositions of coexisting garnet/olivine pairs. In this way, crystal/liquid partition coefficients were obtained even for phases which were not in direct contact with liquid because of thermal migration.

Uncertainties in the partition coefficients shown in Figures 10–16 were determined from Gaussian distributions of the compositions of both the quench liquid phase and the crystalline liquidus phases given in Table 1. In all cases, errors in composition were propagated to errors in D strictly from stan-

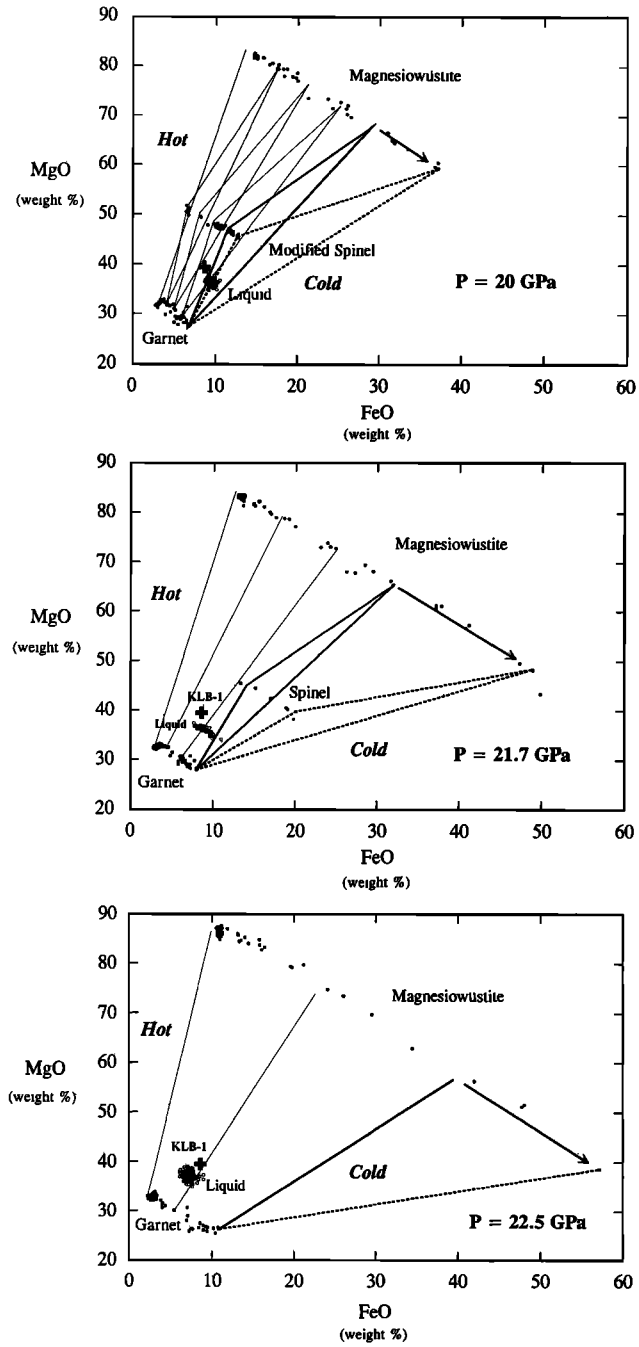

Figure 9. FeO and MgO of phases contained in experiments at 20, 21.7, and 22.5 GPa, KLB1-15, −11, and −36, respectively, of *Zhang and Herzberg* [1994]. Crystallization sequence at 20 GPa is L → L + Gt → L + Gt + Mw → L + Gt + Mw + β → [Gt + Mw + β]. Crystallization sequence at 21.7 GPa is L → L + Gt + Mw → L + Gt + Mw + γ + CaPv → [Gt + Mw + γ + CaPv]. Crystallization sequence at 22.5 GPa is L → L + Mw → L + Mw + Gt → L + Mw + Gt + CaPv → L + Mw + Gt + CaPv + γ → [Mw + Gt + CaPv + γ]. Note the very high FeO contents of coexisting Gt and Mw at the cold ends. Light tie lines are coexisting phases calculated from partition coefficients. Bold solid tie lines are calculated coexisting solidus phases; bold dashed lines are observed coexisting solidus phases. Both calculated and observed solidus phases assemblages are more FeO than KLB-1, demonstrating FeO diffusion to the cold end.

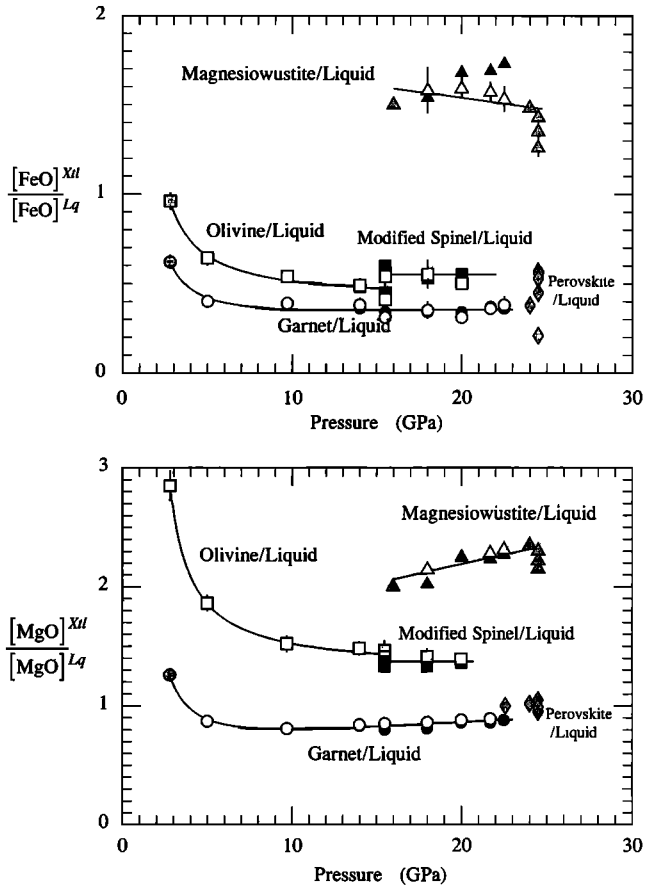

Figure 10. Partition coefficients for FeO and MgO between crystals and liquid. Symbols are defined as follows: open symbols with error bars are partition coefficients determined from average liquidus crystal/liquid analyses; solid symbols are partition coefficients determined from most refractory liquidus crystal/liquid analyses; shaded symbols are results from other workers (2.8 GPa from *Longhi* [1995], 16 GPa from *McFarlane et al.* [1991], 24 GPa from *Ito and Katsura* [1992], and 24.5 GPa from *McFarlane et al.* [1994]); circles are garnet; squares are olivine and modified spinel; triangles are magnesiowustite; diamonds are magnesium perovskite. Data at 14 GPa are from *Zhang and Herzberg* [1994]. Regressions are given in Table 2. Error bars are 1 standard deviation.

dard deviations without correcting for covariance, or nonindependence of the variances. However, visual inspection of Figure 6 shows that the variations in weight percent FeO and MgO for analyzed liquids at 15.5 GPa covary with FeO-MgO systematics for liquidus garnet. This was confirmed by calculating $D_{FeO}^{Gt/Lq}$ from the most refractory garnets and liquids, that is, individual analyses with the lowest FeO/MgO and CaO/Al_2O_3; the result was a D value that was very similar in most cases to partition coefficients that were calculated from the mean values of the garnet and liquid populations. For practical analytical reasons, each individual liquid analysis could not be acquired with a coexisting garnet analysis, and the covariance could not be evaluated by means of a correlation coefficient. Therefore the standard deviations for D could not be reduced, and the values given here should be considered maximum bounds. Crystal/liquid partition coefficients are summarized in Table 2 and illustrated in Figures 10–16. In some cases there

Table 2. Crystal/Liquid Partition Coefficients

	Olivine	Modified Spinel	Anhydrous B Phase	Garnet	Magnesiowustite
TiO_2	A (0.05)	0.12 (0.07)	0.23 (0.13)	0.35 (0.22)	0.27 (0.27)
Al_2O_3	0.04 (0.02)	0.29 (0.07)	0.39 (0.07)	B (0.57)	0.31 (0.05)
Cr_2O_3	C (0.08)	0.62 (0.09)	1.11 (0.17)	D (0.52)	E (0.18)
FeO	F	0.55 (0.05)	0.54 (0.05)	0.35 (0.04)*	G (0.09)
MnO	0.41 (0.29)	0.41 (0.29)	1.47 (1.36)	0.57 (0.47)	0.82 (0.58)
MgO	H	1.37 (0.06)	1.59 (0.09)	I (0.04)*	J (0.07)
CaO	0.03 (0.01)	0.01 (0)	0.01 (0)	K (0.13)	0.01 (0)
Na_2O	0.12 (0.03)†	0.07 (0.04)	0.10 (0.03)	L (0.07)	M (0.16)
NiO	N	1.25 (0.34)	1.31 (0.33)	0.27 (0.12)	3.97 (0.86)

For A, $D = 0.07P$; for B, D = D exp $(-1.213 - 3.22P^{0.5} + 11.09/P^2 + 5.523 \ln P)$; for C, $D = -0.028P + 0.56$; for D, $D = -0.126P + 3.97$; for E, $D = -0.115P + 4.01$; for F, $D = \exp(-0.907 + 2.415/P)$; for G, $D = -0.013P + 1.80$; for H, $D = 1/(0.776 - 1.19P)$; for I, $D = 0.008P + 0.71$; for J, $D = 0.032P + 1.55$; for K, $D = 0.008P + 0.45$; for L, $D = \exp(-5.95 + 0.122P + 0.743 \ln P)$; for M, $D = 0.058P - 0.76$; and for N, $D = -0.012P + 8.3/P + 0.40$. Numbers in parentheses are 1 standard deviation. D, partition coefficient; P, pressure in GPa. D mol %/D wt% conversion factors are 1 for Gt/Lq; 0.94 for Ol/Lq; and 0.84 for Mw/Lq.

*Valid between 14.0 and 22.5 GPa.

†Valid between 10 and 15 GPa.

are important pressure effects, and these have been regressed with empirical equations included in Table 2.

Partition coefficients normalized to liquid also provide a convenient way of calculating the partitioning of cations between crystalline phases. For example, the reader can obtain $D^{Gt/Ol}$ at any pressure from equation (5) together with the values of $D^{Gt/Lq}$ and $D^{Ol/Lq}$ that are retrievable from the empirical equations in Table 2; in a similar way, $D^{Gt/\beta}$ and $D^{Gt/Mw}$ can be easily obtained. Partition coefficients for garnet and clinopyroxene at 5 and 9.7 GPa can be extracted from Tables 2 and 3. The compositions of olivine, modified spinel, spinel, and magnesiowustite that coexist with selected garnets were thus calculated from these intercrystalline partition coefficients, and the results were shown in Figures 4–9. In most cases there is good agreement between observed and calculated phase compositions, and this is especially true near the liquidus where phase compositions have the lowest FeO/MgO. However, we noted above that this agreement breaks down at 20–22.5 GPa for FeO-rich phases that are located near the solidus: observed magnesiowustite and spinel (γ) compositions are always more FeO rich than the calculated ones (Figure 9). These differences arise from nonideal mixing parameters that were ignored in the calculations. *Fei et al.* [1991] show that FeO-MgO mixing in magnesiowustite is highly nonideal, and ignoring the large interaction parameters will result in calculated FeO contents that are lower than observed. These effects were ignored because the mixing properties of majorite garnets are not known; additionally, the FeO-rich phase compositions at 20–22.5 GPa arose from cold-directed thermal migration as discussed above, and we are primarily interested in solidus phases that mass balance with KLB-1.

It is desirable to compare our crystal/liquid partition coefficients with those that are available from other high-pressure experimental determinations [*Kato et al.*, 1988a, b; *Ohtani and Sawamoto*, 1987; *Ohtani et al.*, 1989; *Yurimoto and Ohtani*, 1992; *Ito and Takahashi*, 1987; *Agee*, 1990; *Agee and Walker*, 1990; *Agee et al.*, 1995; *McFarlane et al.*, 1991, 1994; *Drake et al.*, 1993; *Ito and Katsura*, 1992; *Tronnes et al.*, 1992]. However, it has been shown that some partition coefficients determined from experiments on chondrite compositions differ from those of peridotite compositions [*McFarlane et al.*, 1994], and a comprehensive parameterization is not possible at the present time because the data base is not sufficiently broad in T-P-X space. Therefore we have narrowed the focus of these comparisons to only those experiments that have characterized the partial melting properties of mantle peridotite, these being magmas that range in composition from basalt through komatiite and peridotite.

Inspection of Figure 1 shows that major crystalline phase transformations occur in mantle peridotite at pressures in excess of 10 GPa, and it is of great interest to know how these will affect the compositions of magmas. We have therefore plotted our partition coefficients in Figures 10–16 as a function of pressure even though the T-P conditions of our experiments were not isothermal and, as discussed below, temperature is demonstrated to have the dominant effect in some cases.

FeO and MgO

Figure 10 shows D for FeO increases in the order Gt/Lq < Ol/Lq < β/Lq < Mw/Lq, and for most experiments the errors in D (i.e., 1 standard deviation) are about the size of the symbols. Again D values for all elements calculated from both the mean and the most refractory compositions are similar, but those for magnesiowustite/liquid are an important exception. $D_{FeO}^{Mw/Lq}$ calculated from most refractory analyses are usually higher than those calculated from averages, and this is most evident for our highest pressure experiments, those at 21.7–22.5 GPa. These are also experiments which exhibit the largest amount of FeO cold-directed thermal diffusion, but an exact relationship remains uncertain. It should be noted that $D_{FeO}^{Mw/Lq}$ determined from average analyses in this work are in excellent agreement with D values reported at 16–24.5 GPa [*McFarlane et al.*, 1991, 1994; *Ito and Katsura*, 1992].

Figure 10 also shows that D for MgO increases in the order Gt/Lq < β/Lq < Ol/Lq < Mw/Lq. There appears to be a substantial pressure dependency to $D_{MgO}^{Ol/Lq}$ in addition to $D_{FeO}^{Ol/Lq}$, but this is actually a temperature and composition effect; in particular, the MgO contents of the liquids used in this analysis increase from about 17% at 2.8 GPa [*Longhi*, 1995] to about 37% at 14 GPa. The effect of temperature is to drop $D^{Ol/Lq}$ for FeO and MgO because of the enhanced solution of olivine in the silicate melt [e.g., *Roedder and Emslie*, 1970; *Beattie et al.*,

Table 3. Phase Compositions for KLB-1 on the Anhydrous Solidus

T, °C	P, GPa	Phase	Percent Phase	SiO_2	TiO_2	Al_2O_3	Cr_2O_3	FeO	MnO	MgO	CaO	Na_2O	NiO
1726	5	liquid	<1	46.00 (0)	0.44 (0.28)	7.47 (1.70)	0.59 (0.09)	13.19 (1.32)	0.25 (0.21)	21.04 (0.97)	8.15 (2.16)	2.68 (11.85)	0.19 (0.08)
		Ol	63	40.26	0.02	0.35	0.29	9.96	0.12	48.13	0.29	0.13*	0.45
		Gt	10	42.83	0.18	22.00	2.32	6.20	0.17	21.50	4.69	0.05*	0.06
		Cpx	27	54.37	0.1	4.05	0.50	6.01	0.11	25.54	8.5	0.65*	0.11
1968	9.7	liquid	<1	45.00 (5.00)	0.65 (0.41)	3.18 (0.53)	0.35 (0.08)	15.97 (2.33)	0.21 (0.18)	25.40 (2.65)	6.91 (1.81)	2.11 (3.22)	0.21 (0.09)
		Ol	62	40.36	0.06	0.16	0.13	9.99	0.11	48.32	0.26	0.32	0.30
		Gt	19	46.12	0.28	16.34	1.20	6.90	0.15	24.70	4.50	0.12	0.07
		Cpx	19	55.29	0.03	1.76	0.25	5.65	0.17	25.18	9.94	0.74	0.06
2040	14	liquid	<1	45.00 (5.00)	0.98 (0.63)	1.95 (0.33)	0.40 (0.10)	15.79 (2.31)	0.21 (0.17)	25.56 (2.63)	8.41 (2.10)	1.49 (1.03)	0.21 (0.09)
		Ol	60	40.37	0.12	0.10	0.09	9.93	0.11	48.51	0.32	0.23	0.22
		Gt	35	49.30	0.43	9.61	1.11	6.92	0.15	26.3	5.92	0.19	0.07
		Cpx	5	55.74	0.11	1.44	0.28	5.17	0.16	21.94	14.49	1.05	n.a.
2050	15.5	liquid1	<1	45.00 (5.00)	0.43 (0.27)	1.82 (0.32)	0.27 (0.08)	15.55 (2.27)	0.21 (0.17)	25.16 (2.58)	9.45 (2.31)	1.91 (1.02)	0.20 (0.09)
		Ol1	59	40.39	0.06	0.09	0.04	9.92	0.11	48.48	0.37	0.30	0.22
		Gt1	41	49.79	0.19	8.40	0.70	6.90	0.15	26.60	6.88	0.32	0.07
2050	15.5	liquid2	<1	45.00 (5.00)	0.43 (0.27)	1.63 (0.29)	0.24 (0.07)	14.02 (2.04)	0.21 (0.17)	26.23 (2.69)	9.64 (2.35)	2.40 (1.29)	0.21 (0.09)
		Beta2	58	40.03	0.07	0.63	0.2	10.29	0.11	47.97	0.13	0.22	0.34
		Gt2	42	50.30	0.19	7.50	0.62	6.19	0.15	27.60	6.98	0.40	0.07
2160	18	liquid	<1	45.00 (5.00)	0.44 (0.28)	1.99 (0.41)	0.28 (0.08)	14.08 (2.06)	0.21 (0.18)	26.18 (2.68)	9.74 (2.30)	1.87 (0.67)	0.21 (0.09)
		Beta	59	39.99	0.07	0.77	0.23	10.33	0.12	47.84	0.13	0.17	0.35
		Gt	41	50.45	0.19	7.50	0.58	6.05	0.15	27.45	7.10	0.46	0.07
		KLB-1		44.3	0.12	3.54	0.38	8.59	0.14	39.50	3.03	0.30	0.21

Numbers in parentheses are 1 standard deviation. KLB-1 analyses are for the bulk composition [*Zhang and Herzberg*, 1994].
*Residuals for Na_2O at 5 GPa are high.

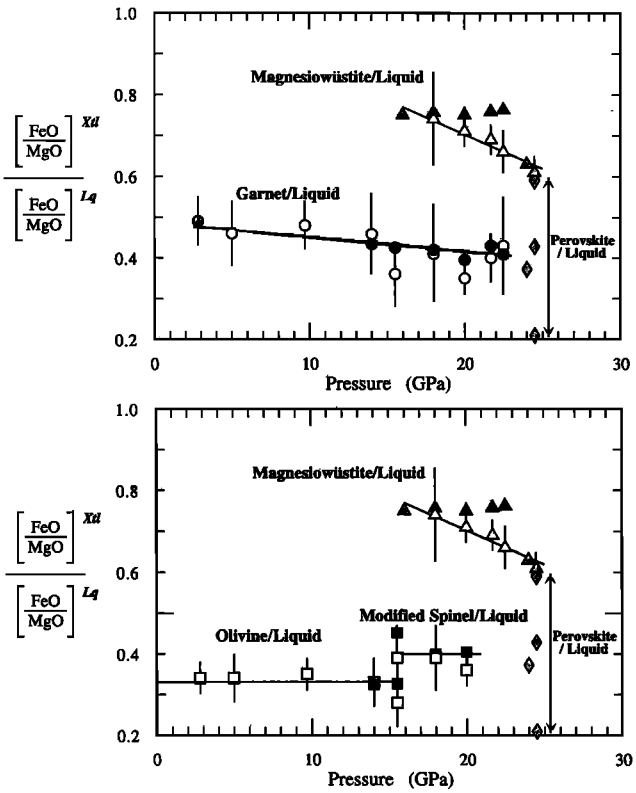

Figure 11. Exchange coefficients of FeO and MgO between crystals and liquid. Symbols are as for Figure 10. Error bars are 2 standard deviations.

1991; *Hirschmann and Ghiorso*, 1994], and the temperature effect will be most pronounced at lower pressures where ΔT for the solidus-liquidus melting interval is greatest. These effects can be minimized by considering simultaneously the partitioning of FeO and MgO, the exchange coefficient [*Beattie et al.*, 1993]:

$$K_{D\mathrm{FeO/MgO}}^{\mathrm{Ol/Lq}} = D_{\mathrm{FeO}}^{\mathrm{Ol/Lq}} \quad (6)$$

$$K_{D\mathrm{FeO/MgO}}^{\mathrm{Ol/Lq}} = [\mathrm{FeO/MgO}]_{\mathrm{Ol}}/[\mathrm{FeO/MgO}]_{\mathrm{Lq}}. \quad (7)$$

Roedder and Emslie [1970] demonstrated that $K_{D\mathrm{FeO/MgO}}^{\mathrm{Ol/Lq}} = 0.30$ for basalts that were saturated in olivine, a value that has been reproduced in many experimental studies since then, and inspection of Figure 11 shows that $K_{D\mathrm{FeO/MgO}}^{\mathrm{Ol/Lq}}$ is 0.33 ± 0.06 (2 standard deviations) from 2.8 to 15.5 GPa, demonstrating a rather remarkable constancy. This seems to hold true for tholeiite, mildly alkaline and komatiitic liquids that are typical of melts generated in the anhydrous peridotite melting interval. *Tronnes et al.* [1992] reported olivine and komatiite compositions from melting experiments at 4–11 GPa, and although not included in Figure 11 for clarity, their results are very similar to the ones shown in Figure 11. However, $K_{D\mathrm{FeO/MgO}}^{\mathrm{Ol/Lq}}$ can be very low (i.e., <0.25) for SiO_2-undersaturated magmas such as nephelinites [*Gee and Sack*, 1988] and for Fe_2SiO_4-rich compositions [*Bowen and Schairer*, 1935; *Agee and Walker*, 1988], and a fully parameterized model remains to be evaluated. The effect of pressure is to increase K_D [*Takahashi and Kushiro*, 1983; *Herzberg*, 1987; *Ulmer*, 1989; *Agee and Walker*, 1988], but again a fully parameterized model remains to be evaluated. The results of our work indicate that the constancy of $K_D^{\mathrm{Ol/Lq}}$ at 0.33 ± 0.06 (2σ) may be due to compensating pressure and composition effects. Indeed, the error bars in our data would permit the interpretation that K_D increases to a maximum of 0.36 at 5–10 GPa (Figure 11) and that it may drop at yet higher pressures. *Agee et al.* [1995] reported $K_D^{\mathrm{Ol/Lq}} = 0.36 \pm 0.09$ for experiments on chondrite at 10 GPa and suggested quench effects as the main source of the error. Our uncertainties are lower, demonstrating the limited contribution to this uncertainty from thermal migration.

$K_{D\ \mathrm{FeO/MgO}}$ increases from 0.33 for olivine/liquid to 0.40 for modified spinel/liquid at 15.5 GPa (Figure 11), reflecting the well-known tendency for modified spinel to be relatively more iron-rich than olivine [*Katsura and Ito*, 1989; *Akaogi et al.*, 1989]. Figure 11 also shows that $K_{D\mathrm{FeO/MgO}}^{\mathrm{Gt/Lq}}$ is about 0.42 ± 0.10 (2σ), and the effect of pressure is to decrease it marginally; this is in good agreement with 0.46 reported by *Agee et al.* [1995] on chondrite, indicating that their more Fe-rich composition bulk composition may have little effect. For $K_{D\mathrm{FeO/MgO}}^{\mathrm{Mw/Lq}}$ the effect of pressure is rather substantial (Figure 11).

We do not have data on magnesium perovskite, but readers should note the wide range of values that have been published for $K_{D\mathrm{FeO/MgO}}^{\mathrm{Pv/Lq}}$ (Figure 11): *McFarlane et al.* [1994] reported values as high as 0.59 in two experiments (i.e., UHP-723 and UHP-892), similar to those between magnesiowustite and liquid; in another experiment they reported a value of 0.43 (i.e., UHP-896), similar to that of *Ito and Katsura* [1992, 0.37]; the value of 0.21 is from *Kato et al.* [1988b]. An evaluation of this problem can be made by examining data for coexisting perovskite-magnesiowustite pairs. The exchange coefficient $K_{D\mathrm{FeO/MgO}}^{\mathrm{Mw/Pv}}$ is >2.0 for inclusions in diamond and in various diamond anvil experiments [*Guyot et al.*, 1988; *Fei et al.*, 1991; *Kesson and FitzGerald*, 1991]; more recently, *Irifune* [1994] determined it to be 1.63 in multianvil experiments at 24 GPa. The melting experiments in Figure 11 yield $K_{D\mathrm{FeO/MgO}}^{\mathrm{Mw/Pv}} = 1.7$ for the data of *Ito and Katsura* [1992] but 1.0 for the data of *McFarlane et al.* [1994]. As it is unlikely that FeO and MgO will partition equally between perovskite and magnesiowustite, we believe that the perovskite data of *McFarlane et al.* [1994] are in error for their experiments UHP-723 and UHP-892. We recommend that the best value for $K_{D\mathrm{FeO/MgO}}^{\mathrm{Pv/Lq}}$ is around 0.4, based on the results of *Ito and Katsura* [1992] and experiment UHP-896 of *McFarlane et al.* [1994]. This would indicate that FeO and MgO partition between majorite garnet and magnesium perovskite about equally (i.e., $K_{D\mathrm{FeO/MgO}}^{\mathrm{Pv/Gt}} = 1$), a result that is consistent with data reported by *Irifune* [1994].

Al_2O_3 and CaO

Partition coefficients for Al_2O_3 are illustrated in Figure 12. $D_{Al_2O_3}$ averages 0.04 for olivine/liquid, in good agreement the results of *Agee and Walker* [1990], and $D_{Al_2O_3}$ jumps up to 0.29 for modified spinel/liquid, similar to previous studies [*Herzberg et al.*, 1990]. $D_{Al_2O_3}$ for garnet/liquid is not intuitively obvious. It increases from about 2 at 2.8 GPa to about 4 at 10 GPa and then drops back to about 2 at 22 GPa. Although not shown for clarity, these results are in good to excellent agreement with the data of *Ohtani et al.* [1989], *Yurimoto and Ohtani* [1992], *Drake et al.* [1993], and *Kato et al.* [1988a], but they are much lower than the results of *Ito and Takahashi* [1987], who determined $D_{Al_2O_3}^{\mathrm{Gt/Lq}}$ to be about 6 at 20 GPa. The large increase at the low-pressure end is determined mainly by the liquid phase which changes from picrite at 2.8 GPa (Al_2O_3 = 13–14% [*Longhi*, 1995]) to komatiite at 4 to 11 GPa (Al_2O_3 = 3.5–9% [this work; *Tronnes et al.*, 1992]). At 14–22.5 GPa the liquids

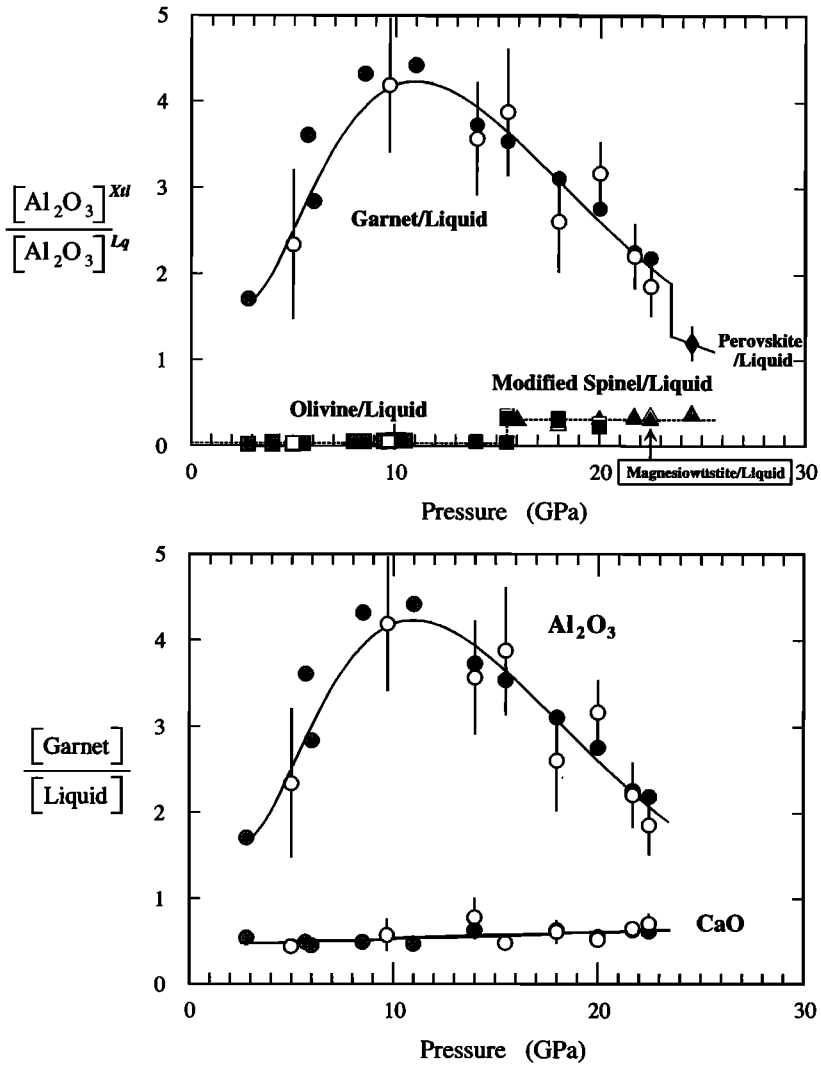

Figure 12. (top) Partition coefficients for Al_2O_3 between various crystalline phases and liquid and (bottom) partition coefficients for Al_2O_3 and CaO between garnet and liquid. Symbols are as for Figure 10, but shaded circles are from *Tronnes et al.* [1992] and *Longhi* [1995]. Regressions are given in Table 2. Error bars are 1 standard deviation.

contain 3–4% Al_2O_3, and the drop in $D_{Al_2O_3}$ is determined mainly by the garnet phase which drops from about 15% Al_2O_3 at 10 GPa to about 7.5% at 22 GPa (Figure 13). It is important to emphasize that the pressure-induced changes in $D_{Al_2O_3}$ shown in Figure 12 are strictly valid for the equilibrium melting of mantle peridotite, and should only be extended to other compositional systems with caution.

Experimental results on magnesium perovskite [*McFarlane et al.*, 1994] yield low D values, and Figure 12 shows that $D_{Al_2O_3}$ drops from about 2 to 1 at the transformation of majorite garnet to magnesium perovskite. This is consistent with other experimental observations that show lower Al_2O_3 in perovskite coexisting with majorite garnet [*Ringwood*, 1991; *Irifune*, 1994].

Figure 12 also shows that $D_{CaO}^{Gt/Lq}$ remains <1 and fairly constant at all pressures. This will be discussed again below, and it is important because it demonstrates that large pressure-induced changes in CaO/Al_2O_3 must occur for liquids generated on the garnet peridotite solidus.

Cr_2O_3

Figure 14 shows that $D_{Cr_2O_3}$ increases at the olivine to modified spinel phase transformation, similar to $D_{Al_2O_3}$. There is a systematic drop in $D_{Cr_2O_3}^{Gt/Lq}$ with increasing pressure, but Cr_2O_3 remains compatible in garnet at all pressures. Figure 14 shows that the lower-pressure data are more scattered about the regression, but these are also lower-temperature data. Experiments at 18–21.7 GPa were all run at about the same temperature, and the effect of pressure in lowering $D_{Cr_2O_3}^{Gt/Lq}$ is unambiguous. There appears to be little change in $D_{Cr_2O_3}$ where majorite garnet transforms to magnesium perovskite. Cr_2O_3 is also compatible in magnesiowustite, and our results are in excellent agreement with previous determinations [*McFarlane et al.*, 1991, 1994].

Na_2O

Na_2O remains incompatible in all the phases studied, but there are some interesting pressure effects as shown in Figure

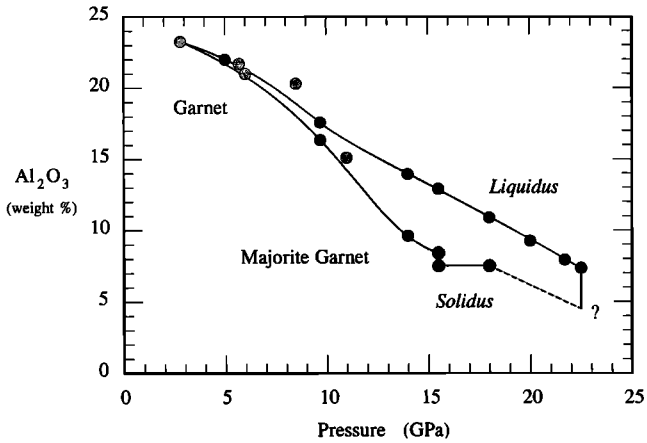

Figure 13. The content of Al_2O_3 in garnet within the melting interval of mantle peridotite. Liquidus garnets of this work (solid circles) at $P > 14$ GPa were calculated from partition coefficients and the KLB-1 bulk composition in order to eliminate the experimental effects of thermal migration but are in good agreement with observed garnets are given in Table 1. Shaded circles are garnets from *Longhi* [1995] at 2.8 GPa and *Tronnes et al.* [1992] at 5.5 to 11 GPa.

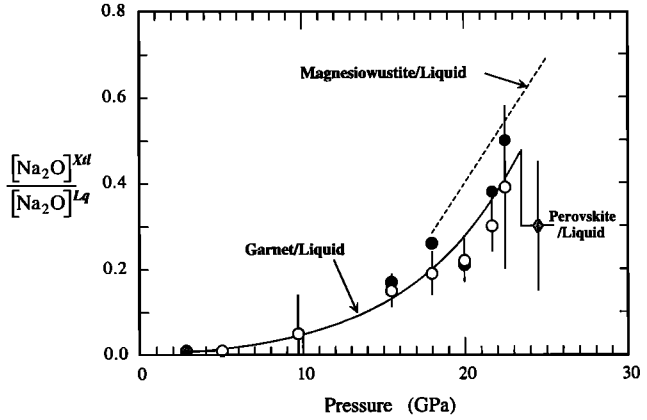

Figure 15. Partition coefficients for Na_2O for garnet/liquid and magnesiowustite/liquid. Regressions are given in Table 2. Error bars are 1 standard deviation.

15. One is to increase $D^{Gt/Lq}_{Na_2O}$ by orders of magnitude from 2.8 to 22.5 GPa, reflecting the stabilization of sodium garnet [*Gasparik*, 1990]. The partitioning of sodium between perovskite and liquid is similar, although the results of *McFarlane et al.* [1994] indicate that there is a drop in D_{Na_2O}. To preserve clarity, we provide only a regression of our data for $D^{Mw/Lq}_{Na_2O}$ in Figure 15. The D values are surprisingly high and the effect of pressure is large. However, we observe no condition in which Na_2O becomes compatible in magnesiowustite, as did *Agee* [1990] on chondrite, indicating the possible operation of important bulk composition controls.

NiO

There is an apparent reduction in $D^{Ol/Lq}_{NiO}$ from 5 to 15.5 GPa as shown in Figure 16, but this is more likely a temperature and composition effect as discussed above for $D^{Ol/Lq}_{MgO}$. Indeed, our results are in excellent agreement with previous work that shows $D^{Ol/Lq}_{NiO}$ is positively correlated with $D^{Ol/Lq}_{MgO}$ [*Jones*, 1984; *Beattie et al.*, 1991; *Hirschmann and Ghiorso*, 1994]. At 15.5 GPa where olivine transforms to modified spinel, NiO changes from being slightly incompatible to slightly compatible. NiO remains incompatible in garnet at all pressures, and D_{NiO} remains constant at the transformation of majorite garnet to perovskite. NiO is strongly compatible in magnesiowustite, and our results for $D^{Mw/Lq}_{NiO}$ are in excellent agreement with previously published results [*McFarlane et al.*, 1991, 1994].

Compositions of Liquids on the Anhydrous Peridotite Solidus

There are a number of difficulties with determining the compositions of liquids on the anhydrous peridotite solidus for small melt fractions (i.e., <5% [*Cawthorn et al.*, 1973; *Baker and Stolper*, 1994]). Chief among them has been modification of the liquid during the quench, a problem that is being examined by segregating the liquid into the pore spaces of a diamond aggregate [*Baker et al.*, 1992, 1995; *Baker and Stolper*, 1994; *Hirose and Kushiro*, 1992, 1993], but most experiments on low melt fractions have been acquired at low pressures where plagioclase and spinel herzolites are the residual crystalline

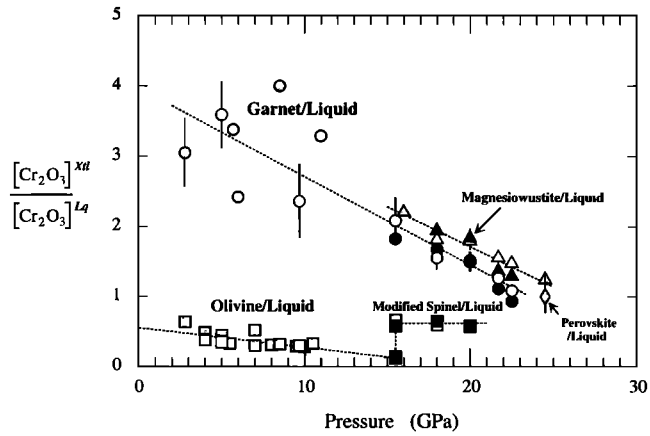

Figure 14. Partition coefficients for Cr_2O_3 between various crystalline phases and liquid. Symbols are as for Figures 10 and 12. Regressions are given in Table 2. Error bars are 1 standard deviation.

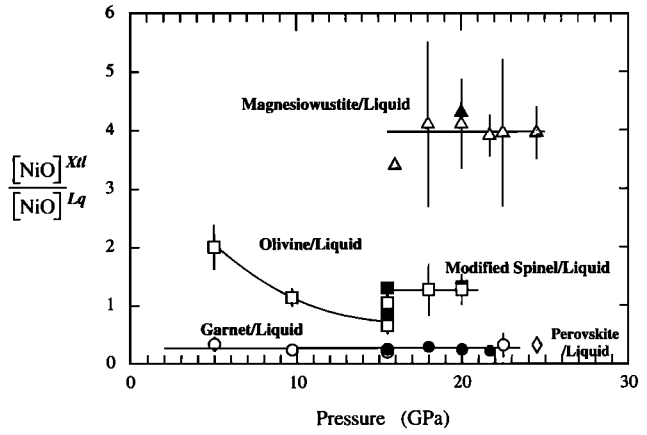

Figure 16. Partition coefficients for NiO between various crystalline phases and liquid. Symbols are as for Figure 10. Regressions are given in Table 2. Error bars are 1 standard deviation.

phases and, with a few exceptions [*Longhi*, 1995] there is a paucity of piston cylinder data at pressures in excess of 2.5 GPa where garnet is stable. Experiments with garnet have largely been acquired with the multianvil apparatus, and these have demonstrated that the compositions of liquids near the peridotite solidus are highly magnesian in the 5–15 GPa range, similar to komatiites [*Herzberg et al.*, 1990; *Wei et al.*, 1990; *Herzberg*, 1992]. However, determinations of liquids at low melt fractions are restricted to parameterized compositions for simplified analogues in CaO-MgO-FeO-Al_2O_3-SiO_2 [*Herzberg*, 1992], and with the exception of recent work by *Walter* [1995], there are few constraints for naturally occurring peridotite. It is important to extend the currently understood melting behavior of the mantle from 2 GPa where it is well known to much higher pressures, and we do this now by calculation. It is emphasized that these calculated liquids are not offered as a substitute for direct experimental observation because there exist large uncertainties for some oxides. However, they will be used in the design of additional experiments in order to lower the levels of uncertainty, and until these improved data are obtained, they will serve as rough estimates of the chemistry of liquids on the anhydrous solidus to pressures extending into the transition zone.

The composition of a crystalline phase can be uniquely determined from partition coefficients and the composition of a liquid because of the constraint of stoichiometry on the chemistry of a crystal. However, a liquid composition cannot be similarly determined from its coexisting crystal because the ratio of metal oxide components to SiO_2 is highly variable in silicate liquids. The SiO_2 content of the liquid must be determined experimentally because thermodynamic estimates [e.g., *Ghiorso and Sack*, 1995] are subject to some uncertainty [*Baker et al.*, 1995]. Pressure-induced shifts in the liquidus crystallization fields of olivine, garnet, and pyroxene, and their peritectic intersections constrain permissable solidus liquid SiO_2 contents [*Herzberg*, 1992]. Pressure tends to increase SiO_2 in FeO-free systems such as CaO-MgO-Al_2O_3-SiO_2, but in natural FeO-bearing systems this increase is offset by the effect of pressure in increasing FeO (see below). The experimental data in FeO-bearing systems indicate that SiO_2 does not change much with pressure in the garnet peridotite stability field, and it is 45–47% in the pressure range 2.5–10 GPa [*Herzberg*, 1992, 1993a, b; also unpublished data, 1996; *Longhi*, 1995; *Walter*, 1995]; furthermore, the experimental data indicate that this relative constancy extends to at least 15 GPa [*Herzberg*, 1992]. We have therefore assumed that the SiO_2 content of liquids on the solidus is 45 ± 5% over the pressure range of 2.5–18 GPa. The ±5% uncertainty is probably too high, but it conservatively encompasses both the experimental database and the spectrum of SiO_2 contents that are observed for naturally occurring picrites and komatiites, even those that formed by advanced melting above the solidus.

The compositions of low degree melts on the solidus ($C_{MO}^{Lq,Sl}$) can now be estimated by rearranging equation (1) to

$$C_{MO}^{Lq,Sl} = [C_{MO}^{Gt,Sl}/D_{MO}^{Gt/Lq}]55/\sum [C_{MO}^{Gt,Sl}/D_{MO}^{Gt/Lq}] \quad (8)$$

for the oxides TiO_2, Al_2O_3, Cr_2O_3, FeO, MnO, MgO, CaO, Na_2O, and NiO; the constant 55 denotes the sum of these oxides given that SiO_2 = 45%. The remaining terms, $C_{MO}^{Gt,Sl}$ and $D_{MO}^{Gt/Lq}$, refer to the composition of the garnet on the solidus and the Gt/Lq partition coefficient, respectively, both of which have been determined in this study (Tables 2 and 3 and Figures 10–16).

Considering for the moment only FeO and MgO for coexisting liquid and olivine on the solidus, equation (8) can be rewritten to

$$C_{FeO}^{Lq,Sl}/C_{MgO}^{Lq,Sl} = [C_{FeO}^{Ol,Sl}/C_{MgO}^{Ol,Sl}][D_{MgO}^{Ol/Lq}/D_{FeO}^{Ol/Lq}] \quad (9)$$

and further rearranged to

$$[C_{FeO}^{Ol,Sl}/C_{MgO}^{Ol,Sl}]/[C_{FeO}^{Lq,Sl}/C_{MgO}^{Lq,Sl}] = [D_{FeO}^{Ol/Lq}/D_{MgO}^{Ol/Lq}] \quad (10)$$

$$[C_{FeO}^{Ol,Sl}/C_{MgO}^{Ol,Sl}]/[C_{FeO}^{Lq,Sl}/C_{MgO}^{Lq,Sl}] = K_{D\,FeO/MgO}^{Ol/Lq} \quad (11)$$

and is equivalent to the exchange coefficient in equation (7). The constancy of $K_{D\,FeO/MgO}^{Ol/Lq}$ over a wide range of temperatures, pressures, and compositions indicates that liquid compositions on the solidus can be calculated with some confidence even though the D values were determined from liquidus crystal/liquid pairs. This is somewhat at variance with the observations of *Baker et al.* [1995], who reported an increase in $K_{D\,FeO/MgO}^{Ol/Lq}$ from 0.25 for Na_2O-rich and SiO_2-rich melts on the solidus to 0.32 for more advanced melting at 1 GPa, but at the higher pressures of interest here, our calculations indicate much more modest changes in Na_2O (see below) and little or no change in SiO_2 with advanced melting (SiO_2 in KLB-1 = 44.30% [*Zhang and Herzberg*, 1994]). Exchange coefficients should therefore be less susceptible to changes in liquid composition in the 5–18 GPa range compared to low pressures where basalts are stable.

Table 3 reports the compositions of crystalline phases that are estimated to occur immediately on the solidus for KLB-1 in the 5–18 GPa range. These were estimated from electron microprobe observations of the crystalline phases located at the cold end of the capsules as discussed above; in most cases the mass balance was good as demonstrated by low residuals between the observed and calculated bulk compositions for KLB-1. These residuals were then lowered by adjusting the observed phase chemistry to correct for the effects of cold-directed thermal migration. An example is shown in Figure 5 for our results at 9.7 GPa; both the measured and optimized contents of FeO and MgO for olivine, garnet, and clinopyroxene at the solidus differ by no more than 1 wt%, but the difference resulted in a more satisfactory mass balance. At 15.5 and 18 GPa there is reasonably good agreement between the observed and optimized phase chemistries as seen in Figures 7 and 8, but at higher pressures, cold-directed thermal migration becomes an increasing problem, as demonstrated by the much higher FeO contents observed for garnet and magnesiowustite at 20–22.5 GPa than is permitted by mass balance (Figure 9). The compositions of liquids on the solidus at 20–22.5 GPa were therefore not estimated.

The weight percent compositions of the first drops of liquid on the anhydrous peridotite solidus were thus calculated, and the results are shown in Figure 17. Errors in the partition coefficients stemming from quench effects and thermal migration were combined with the ±5% uncertainty in SiO_2 at pressures ≥9.7 GPa and propagated to these calculated liquid compositions; errors at 5 GPa are from partition coefficients only, as there is independent evidence that the SiO_2 content of liquids on the solidus is around 46% [*Herzberg*, 1993b]. We have compared our calculated liquids to the low-pressure reference experiments of *Baker and Stolper* [1984] and *Baker et al.* [1995, also personal communication, 1995] at 1 and 2 GPa, and the parameterizations of *Langmuir et al.* [1992] at 2, 3, and 4 GPa. Other experimental data of fine quality [e.g., *Kinzler and*

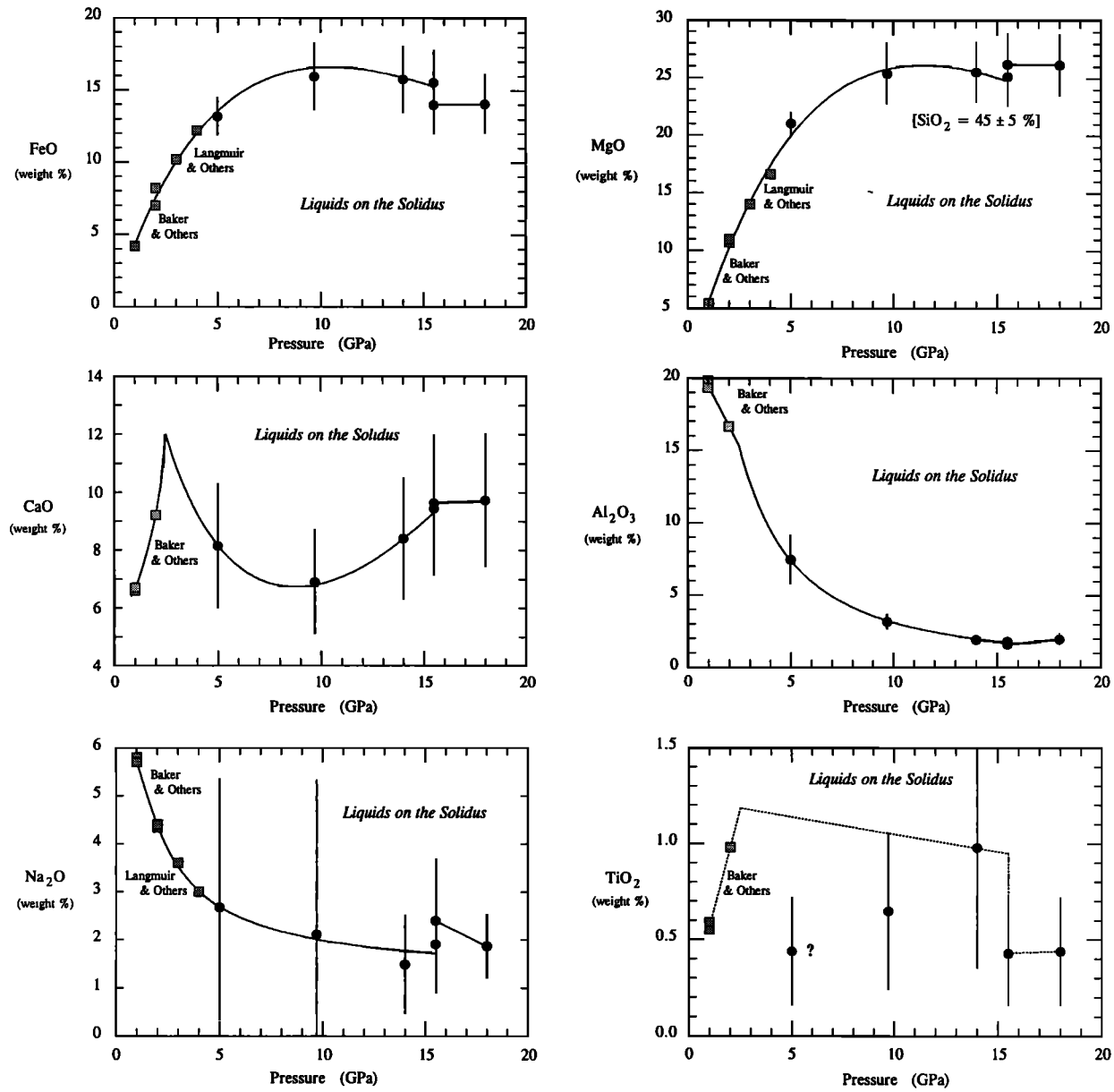

Figure 17. Compositions of liquids on the anhydrous peridotite solidus for KLB-1 at low melt fractions. Regressions are given in the text. Error bars are 1 standard deviation.

Grove, 1992a; *Falloon and Green*, 1987; *Falloon et al.*, 1988; *Takahashi and Kushiro*, 1983; *Fujii and Scarfe*, 1985; *Hirose and Kushiro*, 1993] have not been included because the liquid compositions are strictly valid for higher melt fractions.

Figure 17 shows that the effect of pressure is to increase the content of FeO and MgO, a result that has been known for some time [*O'Hara*, 1968; *Herzberg*, 1992; *Langmuir et al.*, 1992; *Kinzler and Grove*, 1992a; *Takahashi et al.*, 1993; *Hirosh and Kushiro*, 1993]. However, the new results show that there is a maximum concentration for each, this being about 16% FeO and 26% MgO at about 10 GPa. These maxima arise because of the tendency for CaO to increase in the liquid, and this occurs because of the stabilization of majoritic garnet as discussed below. The breaks at 15.5 GPa shown in Figure 17 occur at the transformation of olivine to modified spinel. We have fitted our 5–15.5 GPa data to the 1–4 GPa reference points with the following empirical equations:

$$\mathrm{FeO} = \exp(1.538 - 0.090P + 0.943 \ln P) \quad (12)$$

$$\mathrm{MgO} = \exp(1.800 - 0.089P + 1.018 \ln P) \quad (13)$$

where P is the pressure in gigapascals. Initial liquids develop a komatiite signature with MgO ≥ 18% at pressures in excess of 4 GPa, but MgO is also critically dependent on the content of Na_2O in the liquid as discussed below. These results indicate that komatiites with MgO contents in excess of 26% should be rare, and most of the ones that have been reported were probably affected by olivine accumulation or alteration. However, komatiites have been identified with 28% MgO and a minor olivine phenocryst content [*Arndt*, 1986a; *Nisbet et al.*, 1993]. These elevated MgO contents can be explained by the effects of adiabatic or superadiabatic upwelling [*Langmuir et al.*, 1992; *Steinbach and Yuen*, 1994], by melting of a source region that was depleted in Na_2O as discussed below, or by melting at pressures in excess of 18 GPa.

Figure 17 shows that CaO varies from about 6 to 11% at all pressures. Although it initially drops from 2.5 to about 10 GPa, it tends to increase at higher pressures as clinopyroxene dissolves into garnet. Reference to Table 3 shows that the production of majoritic garnet in this way tends to increase the concentration of CaO in both garnet and clinopyroxene and this is reflected in the liquid. At pressures in excess of 15.5 GPa, all clinopyroxene is dissolved in garnet, and CaO in the liquid becomes fairly constant at about 10%. The pressure function shown in Figure 17 from 2.5 to 15.5 GPa has been fitted to the following empirical equation:

$$\mathrm{CaO} = 31.34 + 2.888P - 0.003P^2 - 16.781P^{0.5} \quad (14)$$

Of all the major elements in magmas, pressure affects the concentration of Al_2O_3 the most; inspection of Figure 17 shows that alumina drops precipitously from about 20% at 1 GPa to about 2% at 15 GPa. This occurs because the effect of pressure is to expand the stability field of garnet and reduce its solubility in silicate liquids [*Herzberg*, 1992, 1995]. The pressure function shown in Figure 17 from 2.5 to 15.5 GPa has been fitted to the following empirical equation:

$$\mathrm{Al_2O_3} = \exp(4.631 - 1.428/P - 1.452 \ln P) \quad (15)$$

Pressure causes a substantial reduction to occur in the content of Na_2O because it becomes increasingly compatible in clinopyroxene [*Langmuir et al.*, 1992; *Blundy et al.*, 1995]; this holds true also at high pressures because Na_2O becomes increasingly compatible in garnet and magnesiowustite (Figure 15). However, at pressures in excess of 5 GPa Na_2O bottoms out at about 2% (Figure 17; although there are large standard deviations in our estimated Na_2O contents, the precision is very good). We emphasize that Na_2O in the liquid will also depend on the Na_2O content of the source region. For KLB-1 this is 0.30%, similar to those in the experiments of *Baker et al.* [1995] (0.31%) and those considered in the parameterizations of *Langmuir et al.* [1992] (0.30%). The pressure function shown in Figure 17 from 1 to 15.5 GPa has been fitted the to following empirical equation:

$$\mathrm{Na_2O} = 1.20 + 8.2/P - 3.65/P^2 \quad (16)$$

The large error at 5–10 GPa reflects the difficulties in constraining $D_{Na_2O}^{Gt/Lq}$ at this pressure range because of the small amounts of Na_2O in garnet. However, our estimates at higher pressures are tighter and indicate that liquids on the solidus will maintain Na_2O contents of around 2%. At 1 GPa, Na_2O reaches nearly 6% and is accompanied by high SiO_2 [*Baker et al.*, 1995]; we believe the lower Na_2O at higher pressures will not impact on our assumption of 45 ± 5% for SiO_2, nor will it affect the estimates in Figure 17.

Our TiO_2 contents are highly uncertain because it is present in KLB-1 at only 0.12%, and our errors are rather large. However, for a peridotite with this composition we estimate that initial liquids on the solidus will contain no more than about 1% TiO_2 at all pressures in the upper mantle and transition zone (Figure 17).

Previous estimates of the compositions of liquids at low melt fractions and at pressures in the 5–10 GPa range were restricted to the system CaO-MgO-FeO-Al_2O_3-SiO_2 [*Herzberg*, 1992]. This was designed in order to reduce the complexity of the system and because komatiites erupt with contents of Na_2O that are typically around 0.5%. However, initial liquids can have about 2% Na_2O even at high pressures (Figure 17),

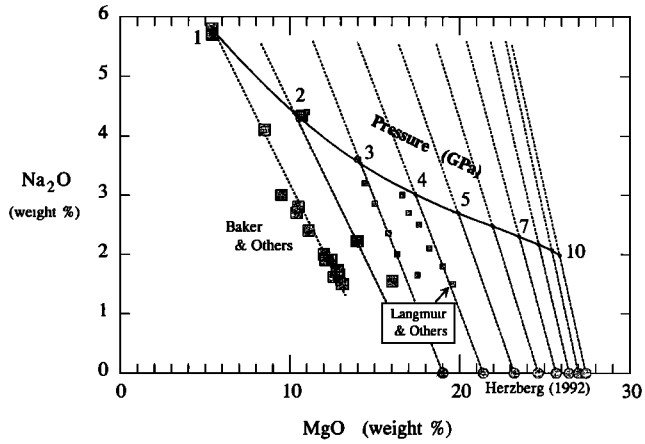

Figure 18. The effect of Na_2O and pressure on the composition of liquids in equilibrium with spinel and garnet lherzolite. Solid line defines the compositions of initial liquids at the pressures indicated for a peridotite source with 0.30 Na_2O, from Figure 17. Dashed lines define the isobaric effect of advanced melting and Na_2O addition on the compositions of liquids in equilibrium with spinel and garnet lherzolite. Key to symbols are large squares, experiments of *Baker and Stolper* [1994], *Baker et al.* [1995] and M. B. Baker (personal communication, 1995); small squares, parameterized liquid compositions of *Langmuir et al.* [1992]; circles, parameterized liquid compositions of *Herzberg* [1992].

and the low contents in komatiite are likely to have resulted from advanced melting during decompression [*Langmuir et al.*, 1992]. An important consequence of advanced melting is that the content of Na_2O drops as MgO increases [*Baker and Stolper*, 1994; *Baker et al.*, 1995; *Langmuir et al.*, 1992; *Kinzler and Grove*, 1992b], and this is demonstrated again in Figure 18. It can be seen that liquids in the system CaO-MgO-FeO-Al_2O_3-SiO_2 are always higher in MgO than the Na_2O-bearing liquids determined in this work, in agreement with the lower pressure studies on basalts. However, Figure 18 shows that these effects are dampened somewhat at high pressures and that the instantaneous change in MgO with Na_2O at the solidus (i.e., $\partial \mathrm{MgO}/\partial \mathrm{Na_2O})_P$ changes from about 2 to 1 as the pressure is increased from 1 to 10 GPa. The effects of adding Na_2O to the source region will also be to create initial liquids with MgO that are lower than those shown in Figure 17.

Depth Estimates of Melt Segregation

The contents of FeO and MgO in a magma are critically dependent on the pressure of melting [*O'Hara*, 1968; *Herzberg*, 1992; *Langmuir et al.*, 1992; *Kinzler and Grove*, 1992a; *Takahashi et al.*, 1993; *Hirosh and Kushiro*, 1993], and this is demonstrated again in Figure 17. There are, however, a number of difficulties with using FeO and MgO as depth indicators. Settling of olivine can affect MgO to the extent that komatiites can fractionate to basalts, and low-pressure fractionation of clinopyroxene and plagioclase can substantially change FeO [*Langmuir et al.*, 1992; *Albarede*, 1992]. For Hawaii, primitive magmas appear to have fractionated along an olivine + clinopyroxene cotectic (L + Ol + Cpx) at pressures in the lithosphere [*Herzberg*, 1995], and this could have modified both FeO and MgO. Finally, source region variations in FeO [*Albarede*, 1992; *Shen and Forsythe*, 1995; *Francis*, 1995; *Scarrow*

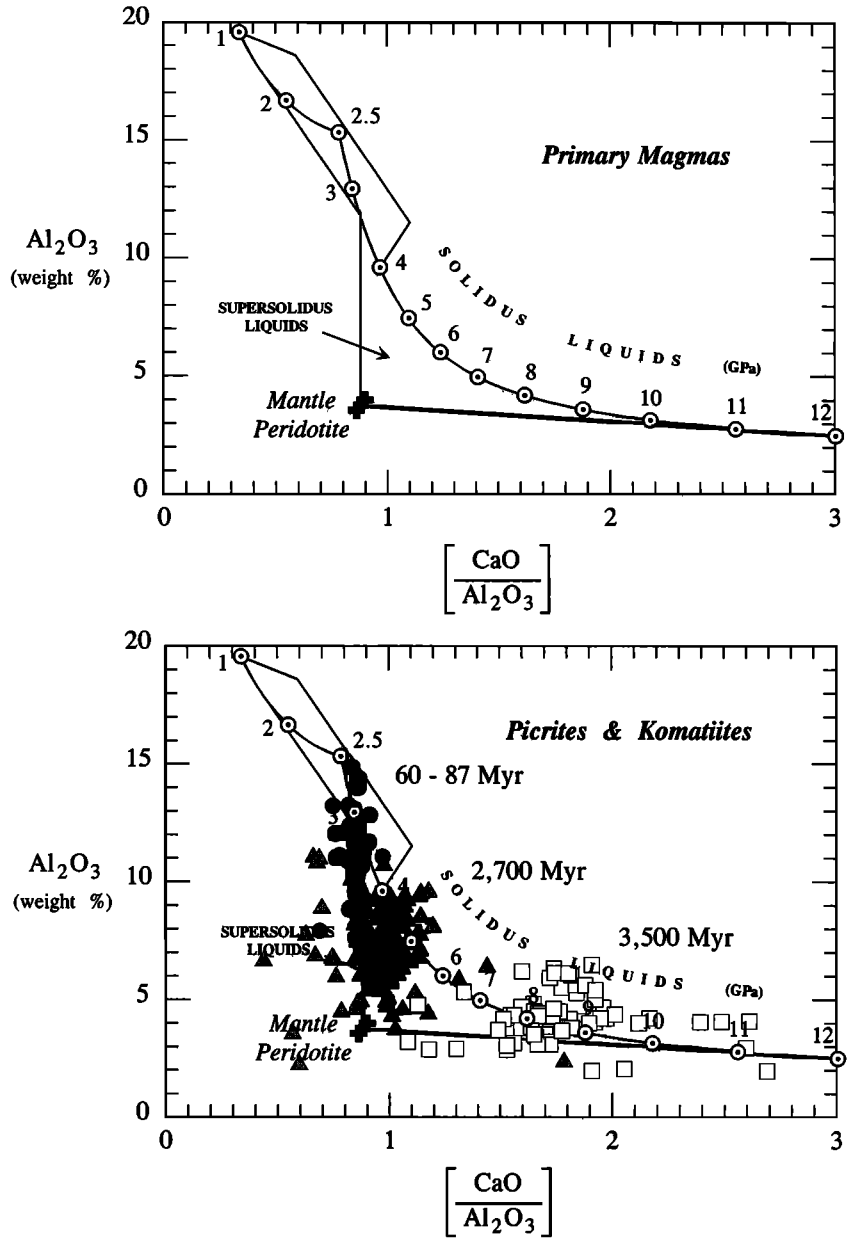

Figure 19. The contents of Al_2O_3 and CaO/Al_2O_3 (top) for primary magmas and (bottom) for picrites and komatiites with the ages shown, modified from *Herzberg* [1995]. Liquids formed along the solidus will have values of Al_2O_3 and CaO/Al_2O_3 indicated by the pressures in gigapascals. Liquids formed by more advanced melting will plot in the shaded area; data at 1–3 GPa are from *Hirosh and Kushiro* [1993], *Baker and Stolper* [1994], *Baker et al.* [1995], and M. B. Baker (personal communication, 1995). Solid crosses are peridotite compositions KLB-1 (this work) and MM3 [*Baker and Stolper*, 1993]. Picrite and komatiite compositions are from data bases listed by *Herzberg* [1992, 1995]. The effect of olivine addition and subtraction is to lower and raise Al_2O_3, respectively, without changing CaO/Al_2O_3. Olivine subtraction may account for 3500 Myr komatiites that plot above the solidus line.

and Cox, 1995] and Na_2O (Figure 18) can add to the problem of inferring pressure from FeO and MgO.

A good indicator of depth in the garnet peridotite field is Al_2O_3 because its content in initial melts drops considerably with increasing pressure [*Herzberg*, 1992, 1995], as was demonstrated in Figure 17. However, because CaO does not change as much, increasing pressure will also elevate CaO/Al_2O_3 in magmas on the solidus. This is shown in Figure 19, a slightly modified version of a prototype that was originally reported by *Herzberg* [1995] based on liquid compositions in the system $CaO\text{-}MgO\text{-}FeO\text{-}Al_2O_3\text{-}SiO_2$ that were constrained with the shotgun experimental method [*Herzberg*, 1992]. Liquids at cotectics and peritectic points can be bracketted by the liquidus phase for a range of bulk compositions, the so-called shotgun technique of *O'Hara* [1968], and the results are in very good agreement with the determinations reported here. Errors in the partition coefficients for CaO and Al_2O_3 between garnet and liquid will propagate to an uncertainty in the estimation of pressure of about ±10% at ≤5 GPa, and ±20% at 10 GPa. Errors at the high-pressure end are therefore serious and stem

from quench effects and thermal migration. Readers should note, however, that the only difference between Figure 19 and its precursor are (1) ratios of CaO/Al_2O_3 that indicated 9–10 GPa in work by *Herzberg* [1995] now plot at 8–9 GPa and are within stated uncertainties in this work and *Herzberg* [1995]; and (2) the compositions of liquids formed by advanced melting of spinel lherzolite at 1 to 2 GPa are incorporated.

Shown in Figure 19 are the contents of Al_2O_3 and CaO/Al_2O_3 for primary magmas generated in the upper mantle and top of the transition zone; these include all magmas formed throughout the melting interval between the anhydrous solidus and the liquidus for a source region that is similar to KLB-1 in composition. The content of Al_2O_3 in a magma can also depend on the source composition, the degree of partial melting, and the amount of olivine fractionated, but for liquids on the solidus, these factors will not affect pressures estimated from CaO/Al_2O_3 [*Herzberg*, 1992, 1995]. Changing Na_2O by 2–3% will have a small effect on CaO/Al_2O_3, based on similar results between this study on KLB-1 and parameterized liquids in the system $CaO-MgO-FeO-Al_2O_3-SiO_2$ [*Herzberg*, 1992]. The effects of H_2O and CO_2 are difficult to assess on a quantitative basis because of the limited database. Experiments on melilite-H_2O at 3 GPa [*Brey and Green*, 1977] and pyrolite-H_2O at 5.5 to 7.7 GPa [*Inoue and Sawamoto*, 1992] indicate that H_2O has no effect on CaO/Al_2O_3. However, experiments on melilite and kimberlite compositions with mixed CO_2 and H_2O volatiles [*Brey and Green*, 1977; *Ringwood et al.*, 1992] show that garnet is stabilized with respect to clinopyroxene, indicating that pressures determined from CaO/Al_2O_3 in anhydrous systems will be too high.

The most important observation to make of Figure 19 is that secular variations in the geochemistry of picrites and komatiites appear to be correlated with depth of melting and melt segregation. Older komatiites appear to have experienced deeper melting; the higher pressures stabilized garnet relative to olivine and pyroxenes, resulting in magmas with lower Al_2O_3 and higher CaO/Al_2O_3 [*Herzberg*, 1992, 1995].

The phase diagram for mantle peridotite shows that deeper melting must occur at higher temperatures in anhydrous systems, and this was used to constrain plume temperatures [*Herzberg*, 1995]. This is shown again in Figure 20. Although temperature variations below oceanic ridges are subject to some uncertainty [*Langmuir et al.*, 1992; *Shen and Forsythe*, 1995; *White and McKenzie*, 1995], a 1400°C potential ridge temperature is adopted for the present-day Earth in order for melting to occur at 2.5 GPa, the minimum pressure needed to stabilize garnet in peridotite as indicated by trace elements in some ocean ridge basalts [*Salters and Hart*, 1989; *Beattie*, 1993]. It can be seen that the 3.1-GPa pressures recorded in the komatiites from Gorgona and picrites from Greenland would have required a potential temperature of about 1500°C, which is only 100°C above ambient mantle below some present-day ridges. Komatiites with 2700 and 3500 Myr ages would have required temperatures that were 300°C and 450°C hotter, respectively, with errors in pressure propagating to an uncertainty of only ±50°C. If the Earth was hotter by 200° at 2700 Myr ago and 300°C at 3500 Myr ago, as suggested by the cooling Earth model of [*Richter*, 1988], then the komatiites of Archean age would have formed in plumes that were hotter than ambient mantle by only about 100°–200°C. The important inference is that komatiite magmas do not require unusually hot conditions to form.

Although a few Munro-type komatiites with 2700 Myr ages have a geochemistry that can be tied to the solidus at 5–7 GPa, most of them have mantle-like CaO/Al_2O_3 and plot well into the supersolidus field, indicating that they segregated from a harzburgite or dunite source (Figure 19). One interpretation is this geochemistry was established by partial melting at 5–7 GPa with melt segregation at considerably reduced pressures [*Herzberg*, 1995]; this would be consistent with the interpretation of secular variations in the depth of melting and melt segregation, but the geochemistry may have been established by partial crystallization rather than partial melting, in which case melting may have commenced at pressures well in excess of 12 GPa, possibly in the transition zone and lower mantle [*Herzberg*, 1995]. This interpretation would indicate a rather uncertain relationship between depth of melting and time, and that plume volcanism 2700 Myr ago may have been about 400°C hotter than *Richter*'s [1988] ambient mantle. Evidence supporting this scenario is presently conjectural but may be found in the high MgO contents of some komatiites from Alexo, Ontario (28% MgO [*Arndt*, 1986a; *Nisbet et al.*, 1993]).

Rare earth element variations in Hawaiian lavas have been used to constrain the most primitive magma compositions [*Feigneson et al.*, 1996], and Figure 21 shows that these liquids plot somewhat below the solidus line in the 3–4 GPa range. The most simple interpretation is that melting was initiated at 3–4 GPa, and the content of Al_2O_3 was lowered by advanced melting during adiabatic decompression. The degree of melting for the tholeiites has been estimated to be 0.25–6.5% by *Sims et al.* [1995] and 1–9% by *Feigenson et al.* [1996]. These primitive lavas are similar to the Gorgona komatiites in having 17–18% MgO and require a potential temperature of 1500°C; this is only about 100°–150°C higher than potential temperatures below some ridges, in good agreement with estimates of *White and McKenzie* [1995].

Komatiites of Cretaceous age have recently been reported from Kamchatka [*Kamenetsky et al.*, 1995], and these are also plotted in Figure 21. There appear to be both low and high alumina types, and the inferred pressures are higher than the Greenland picrites and Gorgona komatiites of comparable age (Figure 19). The low alumina komatiites from Kamchatka define a trend from the 7-GPa solidus liquid composition towards mantle peridotite, and these indicate increased melt fractions. Garnet is the expected residual mineralogy, and this is consistent with depletions in heavy rare earth element (HREE) and high field strength element (HFSE) [*Kamenetsky et al.*, 1995]. If melting was anhydrous, the high pressures inferred from Figure 21 would indicate plume temperatures that were 300°C above ambient mantle, hotter than previous estimates [*Herzberg*, 1995]. However, the Kamchatcka komatiites are located in an arc setting, and the presence of H_2O could have yielded komatiites in cooler plumes.

Meimechites are alkalic komatiites with an abundance of olivine phenocrysts, and the samples plotted in Figure 21 are linked in space and time to the Siberian flood basalts of Permian-Triassic age [*Arndt et al.*, 1995]. They plot close to the solidus line at 9–11 GPa, and their lower Al_2O_3 reflects the abundance of olivine phenocrysts in these rocks. The near-solidus origin is consistent with trace element concentrations, which are high and strongly fractionated [*Arndt et al.*, 1995]. If melting was anhydrous, the high pressures would have required excess temperatures that were 400°–500°C above ambient mantle, again much hotter than previous estimates [*Herzberg*, 1995]. However, small amounts of biotite are common in the

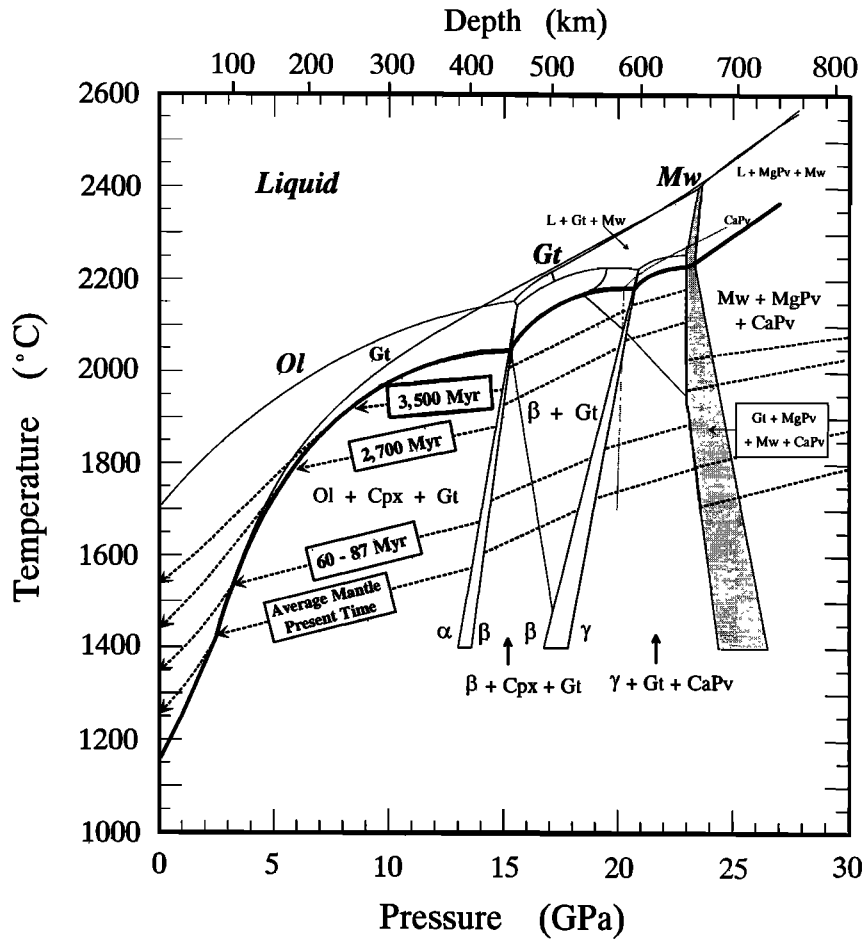

Figure 20. Plume temperatures for anhydrous magmatism inferred from pressure estimates in Figure 19. Adiabatic gradients are modified slightly from *Herzberg* [1995]. Internal plume temperatures refer to the metastable extension of the solid state adiabat to 1 atm, the potential temperature of *McKenzie and Bickle* [1988]. The potential temperature of average mantle below ridges at the present time is about 1400°C.

groundmass of meimechites [*Arndt et al.*, 1995], and the presence of H_2O could have yielded komatiites in cooler plumes.

Ferropicrites from the Boston Creek flow in the Abitibi greenstone belt are Archean in age (~2700 Myr [*Stone et al.*, 1987, 1995a, b; *Xie et al.*, 1993]) and are geochemically similar to those from the Pechenga Complex in the Kola Peninsula of Russia (~2000 Myr [*Hanski*, 1992]). These unusual rocks formed from a source region that was unusually high in FeO/MgO, and they contain trace element concentrations which require the involvement of garnet [*Hansi*, 1992; *Xie et al.*, 1993; *McCuaig et al.*, 1994; *Stone et al.*, 1995b]. However, the major element geochemistry prohibits garnet from being a residual phase [*Hanski*, 1992; *Stone et al.*, 1995a, b], and *Stone et al.* [1995a, b] interpreted these paradoxical observations by the melting of "metasomatically" enriched mantle at low pressures. We examine this model in Figure 21.

The main observation is that most of the ferropicrites have contents of Al_2O_3 and CaO/Al_2O_3 that are actually higher than those of liquids on a high-pressure solidus, and this cannot be explained by olivine fractionation [*Stone et al.*, 1995a, b]. Their removal from the solidus requires that they were formed by advanced melting, but inspection of Figure 21 indicates that the source region must have been fundamentally different from normal mantle peridotite. Advanced melting of normal mantle peridotite would proceed in the following way: [Ol + Cpx + Gt] → {L + Ol + Cpx + Gt} → {L + Ol + Gt} → {L + Ol}; and the liquids would have lower CaO/Al_2O_3 because of the dissolution of garnet (i.e., L + Ol + Gt) as is the case for the Kamchatka komatiites (Figure 21; see discussion of high-pressure phase equilibria by *Herzberg* [1995]). The source region must have been intrinsically high in CaO/Al_2O_3, and we suggest that it was a solidified komatiite. *Hanski* [1992] recommended a mantle source with about 2% Al_2O_3 and 13–15% FeO, and this is similar to a komatiite formed by partial melting at about 10 GPa (Figures 17 and 21). Such a komatiite would have had a garnet trace element signature as long as its primary source was normal mantle peridotite like KLB-1, but pressures higher than 10 GPa may be required to explain the strong depletions in HFSE implied by the majorite garnet signature [*Xie et al.*, 1993; *McCuaig et al.*, 1994]. It is suggested that this komatiite solidified at depth and that it became the source of the ferropicrites. Advanced melting of this unusual source at 4 GPa would yield liquids with pyroxene in the residue instead of garnet, and the liquids would have completely inherited the garnet geochemical signature from the source. Although poorly constrained, the pressures could not have been much higher than about 4 GPa otherwise Al_2O_3 would have been at levels that are lower than observed (Figure 21). The multistage model offered by *Stone et al.* [1995b] is

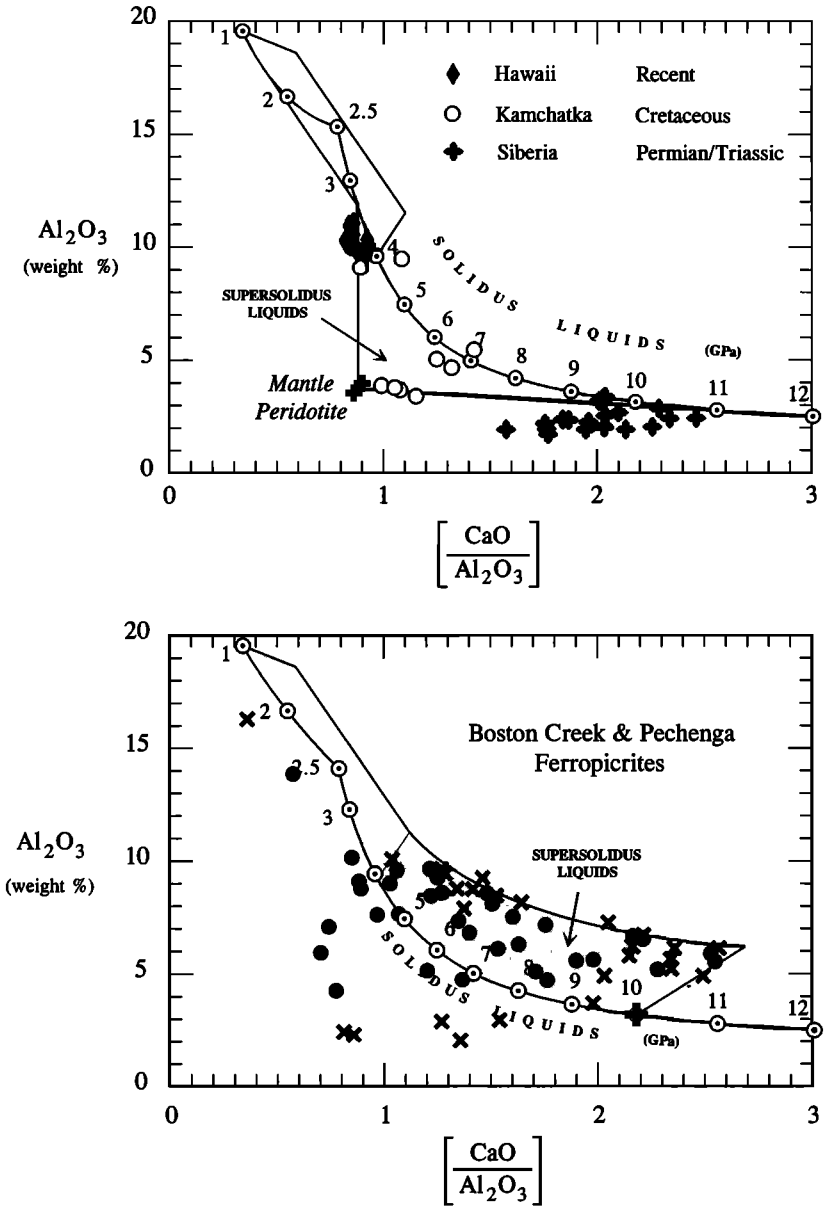

Figure 21. The contents of Al_2O_3 and CaO/Al_2O_3 for basalts from Hawaii [*Feigenson et al.*, 1996], komatiites from Kamchatka [*Kamenetsky et al.*, 1995] and Siberia (i.e., meimechites [*Arndt et al.*, 1995]), and for ferropicrites from the Boston Creek flow of the Abitibi greenstone belt and the Pechenga Complex in the Kola Peninsula. Solid cross (bottom) at 10 GPa is the source composition recommended for the ferropicrites, and is a solidified komatiite. The shaded envelope of high-degree melts of this source is poorly bracketted, but experimental work summarized by *Herzberg* [1992, 1995] indicates that advanced melting at about 4 GPa will proceed in the following way: [Ol + Cpx + Gt] → {L + Ol + Opx + Cpx + Gt} → {L + Ol + Opx + Cpx} → {L + Ol + Opx}; Al_2O_3 will be 5–10%; dissolution of Cpx will increase CaO/Al_2O_3, and dissolution of Opx will lower it. Many ferropicrites have these properties.

similar to this one, except they suggested a metasomatic fluid as the carrier of the garnet signature.

It is noteworthy that many peridotites from alpine-type occurrences in Norway and Switzerland have a komatiite geochemistry: high FeO; low model olivine; and high CaO/Al_2O_3 [*Herzberg*, 1993a]. They are in fact "plutonic" komatiites, or high MgO liquids that failed to erupt to the surface [*Herzberg*, 1993a]. Indeed, the solidification of partial melts at depth may an important process for yielding source regions that can generate Fe-rich magmas [e.g., *Scarrow and Cox*, 1995; *Francis*, 1995] in a subsequent stage of melting.

Discussion

New constraints have been provided on the compositions of liquids that can form on the anhydrous peridotite solidus at low melt fractions and at most pressures in the upper mantle and transition zone. Komatiites are very similar to these experi-

mental compositions except that they are lower in Na_2O and FeO, a difference that could have arisen in part by advanced melting during ascent. Komatiites with primary igneous MgO contents in excess of 26% should be rare, and those that do exist can be explained by advanced melting during adiabatic or superadiabatic ascent, by low Na_2O in the source, or by melting in hot plumes from the transition zone and lower mantle.

Picrites and komatiites display a rich variety of compositions in terms of variable contents of TiO_2, Al_2O_3, MgO, CaO, and Na_2O, and some of these are similar to the liquid variations observed in our high-pressure melting experiments. In particular, the wide range of Al_2O_3 and CaO/Al_2O_3 can be related to the pressure at which melting commences and melt segregation occurs, and this depends critically on internal plume temperature [*Herzberg*, 1992, 1995]. Hot plumes will melt deeper, and the magmas can inherit a high-pressure geochemical signature. Of the high-pressure phases that we have observed from melting experiments on KLB-1 (Figure 1), garnet is most readily identifiable from both trace and major element geochemical criteria [*Sun and Nesbitt*, 1978; *Nesbitt et al.*, 1979; *Jahn et al.*, 1982; *Arndt*, 1986b; *Herzberg*, 1983, 1992, 1995; *Ohtani et al.*, 1989; *Gruau et al.*, 1990; *Yurimoto and Ohtani*, 1992; *Xie et al.*, 1993; *McCuaig et al.*, 1994; *Lecuyer et al.*, 1994; *Lahaye et al.*, 1995; this work]. Most komatiites appear to have experienced melt segregation in the upper mantle and at pressures that ranged from a minimum of 3 GPa to a maximum of about 10 GPa (Figures 19 and 21). These magmas could have formed by anhydrous melting in plumes with temperatures that were only 100°–200°C higher than ambient mantle below ridges. Komatiies do not require unusually hot conditions to form.

Viscous dissipation heating can add to plume temperatures [*Steinbach and Yuen*, 1994], and plumes that ascend through an endothermic phase transformation can increase in temperature because of latent heat effects (i.e., spinel = perovskite + magnesiowustite; Figure 20 [*Steinbach and Yuen*, 1994; *Schubert et al.*, 1995]). Melting within the transition zone or top of the lower mantle may therefore have occurred in the past, but the evidence for this is presently rather ambiguous. The depths of melting for the common Munro-type komatiites with 2700 Myr ages are poorly constrained [*Herzberg*, 1995] (and see above); however, MgO contents in excess of 26% [*Arndt*, 1986a; *Nisbet et al.*, 1993] and mantle-like CaO/Al_2O_3 may be pointing to very deep melting. Evidence for deep melting is also contained in the low-temperature peridotite xenoliths from the lithosphere below the Kaapvaal craton; they have a major element and an isotopic composition that indicate they formed by melting that was much more extensive than is typical of most komatiites (>50% [*Herzberg*, 1993b; *Pearson et al.*, 1995]).

Unfortunately, there are many difficulties associated with characterizing the magmatic products of hot plumes that melt deep. One such ambiguity is that hotter plumes will melt more extensively on their way to the surface, and this can destroy a major element high-pressure signature. However, the trace element contents of komatiites may yield high-pressure signatures where the major elements fail. The effects of majorite garnet removal on depleting such high field strength elements as Nb, Hf, and Zr have now been established for alumina-depleted komatiites [*Xie et al.*, 1993; *McCuaig et al.*, 1994; *Lahaye et al.*, 1995], and additional partitioning experiments may help to place tighter constraints on the depths of melt segregation. However, the effects of perovskite or magnesiowustite fractionation on trace element abundances have not been accurately determined, and komatiites having such a signature have not been unambiguously identified at the present time.

Determining the compositions of liquids formed by low melt fractions on the anhydrous solidus at pressures extending into the transition zone is a difficult but not intractable problem. Most of the uncertainties for FeO and MgO reported here stem from unknown SiO_2 contents of liquids on the solidus, and the assumption that they are 45 ± 5%. For the remaining oxides, the uncertainties arise mostly from quench problems and from thermal migration, with contributions from each being about equal. Estimates of the depths of melt segregation for the Barberton komatiites, which are currently 8–9 GPa, have a possible uncertainty that may be as high as ±20%. The method reported here is therefore not the procedure of choice for determining the chemistry of liquids on the anhydrous solidus, and the calculated liquids are strictly an approximate solution to a difficult problem. However, they are the only estimates that are currently available for pressures extending into the transition zone, and they are in very good agreement with those that have been independently determined on komatiite analogues in more simplified systems [*Herzberg*, 1992]. Indeed, we have performed many additional experiments on komatiite analogues in the system $CaO-MgO-FeO-Al_2O_3-SiO_2$ since our preliminary reports [*Herzberg*, 1992, 1993b], and have encountered fewer problems by using the shotgun technique [*O'Hara*, 1968; *Herzberg*, 1992, 1993b; *Longhi*, 1995]. This method involves bracketting the chemistry of a liquid on the solidus to within several tenths of a weight percent by examining the nature of the liquidus phase for a wide range of known compositions. The drawback is that the shotgun technique is labor intensive, but the number of experiments can be minimized by thoughtfully considering which bulk compositions to select. This is best accomplished by performing experiments on starting materials that are likely to be representative of liquids on the KLB-1 solidus, such as the liquids reported here. These results will be therefore be tested and serve as a compass for directing future experiments to unprecedented levels of accuracy at pressures in the 10–20 GPa range.

Acknowledgments. This research was supported by a grant from the National Science Foundation to Claude Herzberg (EAR 94-06976). The high-pressure experiments were performed at the Stony Brook High Pressure Laboratory, which is part of the NSF Science and Technology Center for High Pressure Research (EAR 89-20239). Special thanks are extended to Michael Baker and John Longhi for providing experimental data prior to publication; Nick Arndt for discussions on komatiites; and Carl Agee, Francois Guyot, and John Jones for thoughtful and constructive reviews. This is Mineral Physics Institute publication 165 at the Department of Earth and Space Sciences, SUNY, Stony Brook.

References

Abbott, D., L. Burgess, and J. Longhi, An empirical thermal history of the Earth's upper mantle, *J. Geophys. Res.*, *99*, 13,835–13,850, 1994.

Agee, C. B., A new look at differentiation of the Earth from melting experiments on the Allende meteorite, *Nature*, *346*, 834–837, 1990.

Agee, C. B., and D. Walker, Static compression and olivine flotation in ultrabasic silicate liquid, *J. Geophys. Res.*, *93*, 3437–3449, 1988.

Agee, C. B., and D. Walker, Aluminum partitioning between olivine and ultrabasic silicate liquid to 6 GPa, *Contrib. Mineral. Petrol.*, *105*, 243–254, 1990.

Agee, C. B., J. Li, M. C. Shannon, and S. Circone, Pressure-temperature phase diagram for the Allende meteorite, *J. Geophys. Res.*, *100*, 17,725–17,740, 1995.

Akaogi, M., E. Ito, and A. Navrotsky, Olivine-modified spinel-spinel transformations in the system Mg_2SiO_4–Fe_2SiO_4: Calorimetric measurements, thermochemical calculation, and geophysical application, *J. Geophys. Res.*, *94*, 15,671–15,685, 1989.

Albarede, F., How deep do common basaltic magmas form and differentiate?, *J. Geophys. Res.*, *97*, 10,997–11,009, 1992.

Arndt, N. T., Differentiation of komatiite flows, *J. Petrol.*, *27*, 279–301, 1986a.

Arndt, N. T., Komatiites: A dirty window to the Archean mantle, *Terra Cognita*, *6*, 59–66, 1986b.

Arndt, N., K. Lehnert, and Y. Vasil'ev, Meimechites: Highly magnesian lithosphere-contaminated alkaline magmas from deep subcontinental mantle, *Lithos*, *34*, 41–59, 1995.

Baker, M. B., and E. M. Stolper, Determining the composition of high-pressure mantle melts using diamond aggregates, *Geochim. Cosmochim. Acta*, *58*, 2811–2827, 1994.

Baker, M. B., S. Newman, J. R. Beckett, and E. M. Stolper, Separating liquid from crystals inn high-pressure melting experiments using diamond aggregates, *Geol. Soc. Am. Abstr. Programs*, *24*, A256, 1992.

Baker, M. B., M. M. Hirschmann, M. S. Ghiorso, and E. M. Stolper, Compositions of near-solidus peridotite melts from experiments and thermodynamic calculations, *Nature*, *375*, 308–311, 1995.

Beattie, P., Uranium-thorium disequilibria and partitioning on melting of garnet peridotite, *Nature*, *363*, 63–65, 1993.

Beattie, P., C. Ford, and D. Russell, Partitioning coefficients for olivine-melt and orthopyroxene-melt systems, *Contrib. Mineral. Petrol.*, *109*, 212–224, 1991.

Beattie, P., M. Drake, J. Jones, W. Leeman, J. Longhi, G. McKay, R. Nielsen, H. Palme, D. Shaw, E. Takahashi, and B. Watson, Terminology for trace-element partitioning, *Geochim. Cosmochim. Acta*, *57*, 1605–1606, 1993.

Blundy, J.D., T. J. Falloon, B. J. Wood, and J. A. Dalton, Sodium, partitioning between clinopyroxene and silicate liquids, *J. Geophys. Res.*, *100*, 15,501–15,515, 1995.

Bowen, N. L., and J. F. Schairer, The system, MgO-FeO-SiO_2, *Am. J. Sci.*, *29*, 151–217, 1935.

Brey, G., and D. H. Green, Systematic study of liquidus phase relations in olivine melilite + H_2O + CO_2 at high pressures and petrogenesis of an olivine melilite magma, *Contrib. Mineral. Petrol.*, *61*, 141–162, 1977.

Canil, D., Orthopyroxene stability along the peridotite solidus and the origin of cratonic lithosphere beneath southern Africa, *Earth Planet. Sci. Lett.*, *111*, 83–95, 1992.

Cawthorn, R. G., C. E. Ford, G. M. Biggar, M. S. Bravo, and D. B. Clarke, Determination of the liquid composition in experimental studies: Discrepancies between microprobe analysis and other methods, *Earth Planet. Sci. Lett.*, *21*, 1–5, 1973.

Chakraborty, W., D. B. Dingwell, and D. C. Rubie, Multicomponent diffusion in ternary silicate melts in the system K_2O-Al_2O_3-SiO_2, II, Mechanisms, systematics, and geological applications, *Geochim. Cosmochim. Acta*, *59*, 265–277, 1995.

Drake, M. J., E. A. McFarlane, T. Gasparik, and D. Rubie, Mg-perovskite/silicate melt and majorite garnet/silicate melt partition coefficients in the system CaO-MgO-SiO_2 at high temperatures and pressures, *J. Geophys. Res.*, *98*, 5427–5431, 1993.

Falloon, T. J., and D. H. Green, Anhydrous partial melting of MORB pyrolite and other peridotite compositions at 10 kbar: Implications for the origin of primitive MORB glasses, *Mineral. Petrol.*, *37*, 181–219, 1987.

Falloon, T. J., D. H. Green, C. J. Hatton, and K. L. Harris, Anhydrous partial melting of a fertile and depleted peridotite from 2 to 30 kb and application to basalt petrogenesis, *J. Petrol.*, *29*, 1257–1282, 1988.

Fei, Y., H.-K. Mao, and B. O. Mysen, Experimental determination of element partitioning and calculation of phase relations in the MgO-FeO-SiO_2 system at high pressure and high temperature, *J. Geophys. Res.*, *96*, 2157–2169, 1991.

Feigenson, M. D., L. C. Patino, and M. J. Carr, Constraints on partial melting imposed by rare earth element variations in Mauna Kea basalts, *J. Geophys. Res.*, in press, 1996.

Francis, D., The implications of picritic lavas for the mantle sources of terrestrial volcanism, *Lithos*, *34*, 61–87, 1995.

Fujii, T., and C. M. Scarfe, Composition of liquids coexisting with spinel lherzolite at 10 kbar and the genesis of MORBs, *Contrib. Mineral. Petrol.*, *90*, 18–28, 1985.

Gasparik, T., Transformation of enstatite-diopside-jadeite pyroxenes to garnet, *Contrib. Mineral. Petrol.*, *102*, 389–405, 1989.

Gasparik, T., Phase relations in the transition zone, *J. Geophys. Res.*, *95*, 15,751–15,769, 1990.

Gee, L, and R. O. Sack, Experimental petrology of melilite nephelinites, *J. Petrol.*, *29*, 1233–1255, 1988.

Ghiorso, M. S., and R. O. Sack, Chemical mass transfer in magmatic processes, IV, A revised and internally consistent thermodynamic model for the interpolation and extrapolation of liquid-solid equilibria in magmatic systems at elevated temperatures and pressures, *Contrib. Mineral. Petrol.*, *119*, 197–212, 1995.

Gruau, G., C. Chauvel, N. T. Arndt, and J. Cornichet, Aluminum depletion in komatites and garnet fractionation in the early Archean mantle: Hafnium isotopic constraints, *Geochim. Cosmochim. Acta*, *54*, 3095–3101, 1990.

Guyot, F., M. Madon, J. Peyronneau, and J. P. Poirer, X-ray microanalysis of high-pressure/high-temperature phases synthesized from natural olivine in a diamond-anvil cell, *Earth Planet. Sci. Lett.*, *90*, 52–64, 1988.

Hanski, E. J., Petrology of the Pechenga ferropicrites and cogenetic, Ni-bearing gabbro-wehrlite intrusions, Kola Peninsula, Russia, *Bull. Geol. Surv. Finl.*, *367*, 192 pp., 1992.

Herzberg, C., Solidus and liquidus temperatures and mineralogies for anhydrous garnet-lherzolite to 15 GPa, *Phys. Earth Planet. Inter.*, *32*, 193–202, 1983.

Herzberg, C., Magma density at high pressure, 2, A test of the olivine flotation hypothesis, in *Magmatic Processes: Physicochemical Principles*, edited by B. O. Mysen, pp. 47–58, Lancaster Press, 1987.

Herzberg, C., Depth and degree of melting of komatiites, *J. Geophys. Res.*, *97*, 4521–4540, 1992.

Herzberg, C. T., Lithosphere peridotites of the Kaapvaal craton, *Earth Planet. Sci. Lett.*, *120*, 13–29, 1993a.

Herzberg, C. T., Magmatism in plumes and hot spots, *Eos Trans. AGU*, *74*(43), Fall Meet. Suppl., 81, 1993b.

Herzberg, C. T., Generation of plume magmas through time: An experimental perspective, *Chem. Geol.*, *126*, 1–18, 1995.

Herzberg, C., T. Gasparik, and H. Sawamoto, Origin of mantle peridotite: Constraints from melting experiments to 16.5 GPa, *J. Geophys. Res.*, *95*, 15,779–15,803, 1990.

Hirose, K., and I. Kushiro, Partial melting of dry peridotites at high pressure: Determination of compositions of melts segregated from peridotite using aggregates of diamonds, *Eos Trans. AGU*, *73*(43), Fall Meet. Suppl., 615, 1992.

Hirose, K., and I. Kushiro, Partial melting of dry peridotites at high pressures: Determination of compositions of melts segregated from peridotite using aggregates of diamond, *Earth Planet. Sci. Lett.*, *114*, 477–489, 1993.

Hirschmann, M. M., and M. S. Ghiorso, Activities of nickel, cobalt, and manganese silicates in magmatic liquids and applications to olivine/liquid and to silicate/metal partitioning, *Geochim. Cosmochim. Acta*, *58*, 4109–4126, 1994.

Inoue, T., and H. Sawamoto, High pressure melting of pyrolite under hydrous condition and its geophysical implications, in *High-Pressure Research: Application to Earth and Planetary Sciences*, *Geophys. Monogr. Ser.*, vol. 39, edited by Y. Syono and M. H. Manghnani, pp. 323–331, AGU, Washington, D. C., 1992.

Irifune, T., Absence of an aluminous phase in the upper part of the Earth's lower mantle, *Nature*, *370*, 131–133, 1994.

Ita, J., and L. Stixrude, Petrology, elasticity, and composition of the mantle transition zone, *J. Geophys. Res.*, *97*, 6849–6866, 1992.

Ito, E., and T. Katsura, Melting of ferromagnesian silicates under the lower mantle conditions, in *High-Pressure Research: Application to Earth and Planetary Sciences*, *Geophys. Monogr. Ser.*, vol. 39, edited by Y. Syono and M. H. Manghnani, pp. 315–322, AGU, Washington, D. C., 1992.

Ito, E., and E. Takahashi, Melting of peridotite under the lower mantle condition, *Nature*, *328*, 514–517, 1987.

Jahn, B.-M., G. Gruau, and A. Y. Glikson, Komatiites from the Onverwacht Group, S. Africa: REE geochemistry, Sm/Nd age and mantle evolution, *Contrib. Mineral. Petrol.*, *80*, 25–40, 1982.

Jochum, K. P., N. T. Arndt, and A. W. Hofmann, Nb-Th-La in komatiites and basalts: Constraints on komatiite petrogenesis and mantle evolution, *Earth Planet. Sci. Lett.*, *107*, 272–289, 1991.

Jones, J. H., Temperature- and pressure-independent correlations of olivine/liquid partition coefficients and their applications to trace element partitioning, *Contrib. Mineral. Petrol.*, *88*, 126–132, 1984.

Kamenetsky, V. S., A. V. Sobolev, J.-L. Joron, and M. P. Semet, Petrology and geochemistry of Cretaceous ultramafic volcanics from Eastern Kamchatka, *J. Petrol.*, *36*, 637–662, 1995.

Kato, T., A. E. Ringwood, and T. Irifune, Experimental determination of element partitioning between silicate perovskites, garnets and liquids: Constraints on early differentiation of the mantle, *Earth Planet. Sci. Lett.*, *89*, 123–145, 1988a.

Kato, T., A. E. Ringwood, and T. Irifune, Constraints on element partition coefficients between $MgSiO_3$ perovskite and liquid determined by direct measurements, *Earth Planet. Sci. Lett.*, *90*, 65–68, 1988b.

Katsura, T., and E. Ito, The system Mg_2SiO_4-Fe_2SiO_4 at high pressures and temperatures: Precise determination of stabilities of olivine, modified spinel, and spinel, *J. Geophys. Res.*, *94*, 15,663–15,670, 1989.

Kesson, S. E., and J. D. Fitz Gerald, Partitioning of MgO, FeO, NiO, MnO and Cr_2O_3 between magnesian silicate perovskite and magnesiowustite: Implications for the origin of inclusions in diamond and the composition of the lower mantle, *Earth. Planet. Sci. Lett.*, *111*, 229–240, 1991.

Kinzler, R. J., and T. L. Grove, Primary magmas of mid-ocean ridge basalts, 1, Experiments and methods, *J. Geophys. Res.*, *97*, 6885–6906, 1992a.

Kinzler, R. J., and T. L. Grove, Primary magmas of mid-ocean ridge basalts, 2, Applications, *J. Geophys. Res.*, *97*, 6907–6926, 1992b.

Lahaye, Y., N. Arndt, G. Byerly, C. Chauvel, S. Fourcade, and G. Gruau, The influence of alteration on the trace-element and Nd isotopic compositions of komatiites, *Chem. Geol.*, *126*, 43–64, 1995.

Langmuir, C. H., E. M. Klein, and T. Plank, Petrological systematics of mid-ocean ridge basalts: Constraints on melt migration beneath ocean ridges, in *Mantle Flow and Melt Generation at Mid-Ocean Ridges*, *Geophys. Monogr. Ser.*, vol. 71, edited by J. Phipps Morgan, D. K. Blackman, and J. Sinton, pp. 183–280, AGU, Washington, D. C., 1992.

Lecuyer, C., G. Gruau, C. R. Anhaeusser, and S. Fourcade, The origin of fluids and the effects of metamorphism on the primary chemical compositions of Barberton komatiites: New evidence from geochemical (REE) and isotopic (Nd, O, H, $^{39}Ar/^{40}Ar$) data, *Geochim. Cosmochim. Acta*, *58*, 969–984, 1994.

Lesher, C. E., and D. Walker, Solution properties of silicate liquids from thermal diffusion experiments, *Geochim. Cosmochim. Acta*, *50*, 1397–1411, 1986.

Lesher, C. E., and D. Walker, Cumulate maturation and melt migration in a temperature gradient, *J. Geophys. Res.*, *93*, 10,295–10,311, 1988.

Liebermann, R. C., and Y. Wang, Characterization of sample environment in a uniaxial split-sphere apparatus, in *High-Pressure Research: Application to Earth and Planetary Sciences*, *Geophys. Monogr. Ser.*, vol. 39, edited by Y. Syono and M. H. Manghnani, pp. 19–31, AGU, Washington, D. C., 1992.

Longhi, J., Liquidus equilibria of some primary lunar and terrestrial melts in the garnet stability field, *Geochim. Cosmochim. Acta*, *59*, 2375–2386, 1995.

McCuaig, T. C., R. Kerrich, and Q. Xie, Phosphorous and high field strength element anomalies in Archean high-magnesian magmas as possible indicators of source mineralogy and depth, *Earth Planet. Sci. Lett.*, *124*, 221–239, 1994.

McFarlane, E. A., M. J. Drake, and C. T. Herzberg, Magnesiowüstite/melt and majorite/melt partitioning and the early thermal history of the Earth (abstract), *Proc. Lunar Planet. Sci. Conf.*, *22*, 875–876, 1991.

McFarlane, E. A., M. J. Drake, and D. C. Rubie, Element partitioning between Mg-perovskite, magnesiowustite, and silicate melt at conditions of the Earth's mantle, *Geochim. Cosmochim. Acta*, *58*, 5161–5172, 1994.

McKenzie, D., and M. J. Bickle, The volume and composition of melt generated by extension of the lithosphere, *J. Petrol.*, *29*, 625–679, 1988.

Nesbitt, R. W., S.-S. Sun, and A. C. Purvis, Komatiites: Geochemistry and genesis, *Can. Mineral.*, *17*, 165–186, 1979.

Nisbet, E. G., M. J. Cheadle, N. T. Arndt, and M. J. Bickle, Constraining the potential temperature of the Archaean mantle: A review of the evidence from komatiites, *Lithos*, *30*, 291–307, 1993.

O'Hara, M. J., The bearing of phase equilibria studies in synthetic and natural systems on the origin and evolution of basic and ultrabasic rocks, *Earth Sci. Rev.*, *4*, 69–133, 1968.

Ohtani, E., Melting relation of Fe_2SiO_4 up to about 200 kbar, *J. Phys. Earth*, *27*, 189–208, 1979.

Ohtani, E., and H. Sawamoto, Melting experiment on a model chondritic mantle composition at 25 GPa, *Geophys. Res. Lett.*, *14*, 733–736, 1987.

Ohtani, E., T. Kato, and H. Sawamoto, Melting of a model chondritic mantle to 20 GPa, *Nature*, *322*, 352–353, 1986.

Ohtani, E., I. Kawabe, J. Moriyama, and Y. Nagata, Partitioning of elements between majorite garnet and melt and implications for petrogenesis of komatiite, *Contrib. Mineral. Petrol.*, *103*, 263–269, 1989.

Pearson, D. G., R. W. Carlson, S. B. Shirey, F. R. Boyd, and P. H. Nixon, The stabilization of Archaean lithospheric mantle: A Re-Os isotopic study of peridotite xenoliths from the Kaapvaal craton, *Earth Planet. Sci. Lett.*, *134*, 341–357, 1995.

Presnall, D. C., and T. Gasparik, Melting of enstatite ($MgSiO_3$) from 10 to 16.5 GPa and the forsterite (Mg_2SiO_4)–majorite ($MgSiO_3$) eutectic at 16.5 GPa: Implications for the origin of the mantle, *J. Geophys. Res.*, *95*, 15,771–15,778, 1990.

Richter, F. M., A major change in the thermal state of the Earth at the Archaean-Proterozoic Boundary: Consequences for the nature and preservation of continental lithosphere, *J. Petrol., Special Lithosphere Issue*, 39–52, 1988.

Ringwood, A. E., Phase transformations and their bearing on the constitution and dynamics of the mantle, *Geochim. Cosmochim. Acta*, *55*, 2083–2110, 1991.

Ringwood, A. E., S. E. Kesson, W. Hibberson, and N. Ware, Origin of kimberlites and related magmas, *Earth Planet. Sci. Lett.*, *113*, 521–538, 1992.

Roedder, P. L., and R. F. Emslie, Olivine-liquid equilibrium, *Contrib. Mineral. Petrol.*, *29*, 275–289, 1970.

Salters, V. J. M., and S. Hart, The hafnium paradox and the role of garnet in the source of mid-ocean-ridge basalts, *Nature*, *342*, 420–422, 1989.

Scarrow, J. H., and K. G. Cox, Basalts generated by decompressive adiabatic melting of a mantle plume: A case study from the Isle of Skye, N. W. Scotland, *J. Petrol.*, *36*, 3–22, 1995.

Schubert, G., C. Anderson, and P. Goldman, Mantle plume interaction with an endothermic phase change, *J. Geophys. Res.*, *100*, 8245–8256, 1995.

Shen, Y., and D. W. Forsyth, Geochemical constraints on initial and final depths of melting beneath mid-ocean ridges, *J. Geophys. Res.*, *100*, 2211–2237, 1995.

Sims, K. W. W., D. J. DePaolo, M. T. Murrell, W. S. Baldridge, S. J. Goldstein, and D. A. Clague, Mechanisms of magma generation beneath Hawaii and mid-ocean ridges: Uranium/thorium and samarium/neodymium isotopic evidence, *Science*, *267*, 508–512, 1995.

Steinbach, V., and D. Yuen, Melting instabilities in the transition zone, *Earth Planet. Sci. Lett.*, *127*, 67–75, 1994.

Stone, W. E., L. S. Jensen, and W. R. Church, Petrography and geochemistry of an unusual Fe-rich basaltic komatiite from Boston Township, northeastern Ontario, *Can. J. Earth Sci.*, *24*, 2537–2550, 1987.

Stone, W. E., J. H. Crocket, and M. E. Fleet, Differentiation processes in an unusual iron-rich alumina-poor Archean ultramafic/mafic igneous body, Ontario, *Contrib. Mineral. Petrol.*, *119*, 287–300, 1995a.

Stone, W. E., J. H. Crocket, A. P. Dicken, and M. E. Fleet, Origin of Archean ferropicrites: geochemical constraints from the Boston Creek flow, Abitibi greenstone belt, Ontario, Canada, *Chem. Geol.*, *121*, 51–71, 1995b.

Sun, S.-S., and R. W. Nesbitt, Petrogenesis of Archaean ultrabasic and basic volcanics: Evidence from rare earth elements, *Contrib. Mineral. Petrol.*, *65*, 301–325, 1978.

Takahashi, E., Melting of a dry peridotite KLB-1 up to 14 GPa: Implications on the origin of peridotitic upper mantle, *J. Geophys. Res.*, *91*, 9367–9382, 1986.

Takahashi, E., and I. Kushiro, Melting of a dry peridotite at high pressures and basalt magma genesis, *Am. Mineral.*, *68*, 859–879, 1983.

Takahashi, E., T. Shimazaki, Y. Tsuzaki, and H. Yoshida, Melting study of a peridotite KLB-1 to 6.5 GPa, and the origin of basaltic magmas, *Philos. Trans. R. Soc. London A*, *342*, 105–120, 1993.

Tronnes, R. G., D. Canil, and K. Wei, Element partitioning between silicate minerals and coexisting melts at pressures of 1–27 Gpa, and implications for mantle evolution, *Earth Planet. Sci. Lett.*, *111*, 241–255, 1992.

Ulmer, P., The dependence of the Fe^{2+}-Mg cation partitioning between olivine and basaltic liquid on pressure, temperature and composition: An experimental study to 30 kbars, *Contrib. Mineral. Petrol.*, *101*, 261–273, 1989.

Walker, D., and C. Agee, Partitioning "equilibrium," temperature gradients, and constraints on Earth differentiation, *Earth Planet. Sci. Lett.*, *96*, 49–60, 1989.

Walker, D., and S. E. DeLong, Soret separation of Mid-Ocean Ridge Basalt magma, *Contrib. Mineral. Petrol.*, *79*, 231–240, 1982.

Walter, M. J., Melting reactions of fertile garnet peridotite, *Eos Trans. AGU*, *76*(17), Spring Meet. Suppl., S297, 1995.

Wei, K., R. G. Tronnes, and C. M. Scarfe, Phase relations of aluminum-undepleted and aluminum-depleted komatiites at pressures of 4 to 1 GPa, *J. Geophys. Res.*, *95*, 15,817–15,828, 1990.

White, R. S., and D. McKenzie, Mantle plumes and flood basalts, *J. Geophys. Res.*, *100*, 17,543–17,585, 1995.

Xie, Q., R. Kerrich, and J. Fan, HFSE/REE fractionations recorded in three komatiite-basalt sequences, Archean Abitibi greenstone belt: Implications for multiple plume sources and depths, *Geochim. Cosmochim. Acta*, *57*, 4111–4118, 1993.

Yurimoto, H., and E. Ohtani, Element partitioning between majorite and liquid: A secondard ion mass spectrometric study, *Geophys. Res. Lett.*, *19*, 17–20, 1992.

Zhang, J., and C. Herzberg, Melting experiments on anhydrous peridotite KLB-1 from 5.0 to 22.5 GPa, *J. Geophys. Res.*, *99*, 17,729–17,742, 1994.

Zhang, Y., D. Walker, and C. E. Lesher, Diffusive crystal dissolution, *Contrib. Mineral. Petrol.*, *102*, 492–513, 1989.

C. Herzberg, Rutgers University, Department of Geological Sciences, Wright-Rieman Laboratories, Busch Campus, New Brunswick, NJ 08903. (e-mail: herzberg@gandalf.rutgers.edu)

J. Zhang, Center for High Pressure Research, State University of New York at Stony Brook, Stony Brook, NY 11794.

(Received August 14, 1995; revised December 22, 1995; accepted January 5, 1996.)